SiO_2 as a Starting Material for the Synthesis of Pentacoordinate Silicon Complexes. 1

K. Y. Blohowiak,[‡] D. R. Treadwell,[†] B. L. Mueller,[†] M. L. Hoppe,[†] S. Jouppi,[†] P. Kansal,[†] K. W. Chew,[†] C. L. S. Scotto,[†] F. Babonneau,[§] J. Kampf,[†] and R. M. Laine*[,†,‡]

Department of Materials Science and Engineering and Department of Chemistry, University of Michigan, Ann Arbor, Michigan 48109-2136; The Department of Materials Science and Engineering and the Polymeric Materials Laboratory of the Washington Technology Center, University of Washington, Seattle, Washington 89195; and Laboratoire de Chimie Matière Condensée, URA CNRS 1466, Université Pierre et Marie Curie, Paris, France

Received August 3, 1994[⊗]

SiO_2 as silica gel, fused silica, or quartzite will react readily in ethylene glycol (EG) with 1 equiv of alkali (M) hydroxide (except Na) to produce, in essentially quantitative yield, monomeric pentacoordinate glycolato silicates [$M(OCH_2CH_2O)_2SiOCH_2CH_2OH$] containing two bidentate glycol ligands and one monodentate ligand. On heating, one EG is lost per two monomer units forming dimeric species, [$M_2Si_2(OCH_2CH_2O)_5$], or polymers, [$MSi(OCH_2CH_2O)_{2.5}]_x$. The Na derivative precipitates out of solution as the dimer. In experiments run with fused silica, the dissolution process exhibits a first-order dependence on base concentration and silica surface area. The E_a for silica dissolution is 14 ± 2 kcal/mol with $\Delta H^{\ddagger} \approx 11$ kcal/mol and $\Delta S^{\ddagger} \approx -44$ cal/mol K. In the absence of base, the silica surface reacts with EG to form an alkoxy-modified surface as determined by diffuse reflectance FTIR spectroscopy (DRIFTS). In the presence of base, only hydroxyl groups are seen on the silica surface. A mechanism for dissolution is proposed based on these observations. The dissolution process appears to be relevant to the nonaqueous synthesis of zeolites, especially silica-sodalite (ZSM-5), which are prepared under very similar conditions. The monomeric, anionic glycolato silicates exhibit trigonal-bipyramidal geometry, with no apparent contact interactions between the anionic framework and the alkali metal counterions. The monomers, dimers and polymers are characterized by chemical analysis, X-ray powder diffractometry, FTIR, solution and solid-state MAS ^{29}Si NMR, and thermal gravimetric analysis. The monomers dissolve readily in methanol but appear to do so via a ligand-exchange process wherein some of the glycolato ligands are displaced by methoxy ligands. On heating, the dimers/polymers decompose to phase-pure alkali silicates.

Introduction

Despite the numerous structural and bonding analogies that can be drawn between silicon chemistry and carbon chemistry, the quantity of published literature in silicon chemistry falls far short of that found for carbon chemistry. Although there are many reasons for this disparity, in part, it reflects the extensive variety of simple carbon-based compounds (feedstock chemicals) derived from petroleum, coal, or biological sources that are available for elaboration for which there are no silicon counterparts.

The primary silicon-based feedstock chemicals derive from two relatively mature processes.[1,2] The first, the dissolution of SiO_2 in strong base, provides access to a wide variety of inorganic silicates, as illustrated in reaction 1.[2] The second, carbothermal reduction of SiO_2

$$SiO_2 + xMOH\ (M = \text{alkali metal}) \xrightarrow{-H_2O} \underset{x=2 \quad x=4}{M_2SiO_3,\ M_4SiO_4} \text{ and others} \quad (1)$$

$$SiO_2 + 2C \xrightarrow{1200\ ^\circ C} 2CO + Si_{met} \quad (2)$$

to metallurgical grade silicon (Si_{met}), reaction 2,[1] provides access to organosilicon compounds via reaction of Si_{met} with alkyl or aryl chlorides (most typically MeCl) in the presence of a catalyst:[1]

$$MeCl + Si \xrightarrow{Cu/Sn\ catalyst\ 200-350\ ^\circ C} MeSiCl_3 + Me_2SiCl_2 + \ldots \quad (3)$$

Alternately, Si_{met} is reacted with a variety of oxidants to prepare related products. For example, reaction with HCl provides[1]

$$HCl + Si \rightarrow H_2 + HSiCl_3 + SiCl_4 \quad (4)$$

† University of Michigan.
‡ University of Washington.
§ Université Pierre et Marie Curie.
* Address correspondence to this author at the University of Michigan.
⊗ Abstract published in *Advance ACS Abstracts,* September 15, 1994.
(1) *Kirk-Othmer Encyclopedia of Chemical Technology,* 3rd ed.; Wiley-Interscience: New York, 1979; Vol. 20, pp 750–880.
(2) Iler, R. K. *The Chemistry of Silica*; John Wiley & Sons: New York, 1979.

0897-4756/94/2806-2177$04.50/0

$SiCl_4$ is a feedstock for the preparation of $Si(OEt)_4$. $HSiCl_3$ is the primary source of electronics grade Si metal:

$$HSiCl_3 + H_2 \xrightarrow{\text{hot wire}} Si_{el} + 3HCl \qquad (5)$$

These reactions, when combined with several more specialized reactions (e.g., hydrosilylation), comprise the basic (and limited) repertoire of the silicon feedstock chemicals industry. Furthermore, because this repertoire is technologically mature, it is unlikely that there will be major changes in or adaptions of these routes that will markedly change the types of compounds produced. Thus, efforts to develop routes to silicon feedstock chemicals are more likely to succeed if they rely on novel approaches rather than on investments in the above, well-developed areas.

The widespread availability of SiO_2 and its extremely low cost continue to make it the most ideal starting point for any new route(s) to silicon feedstock chemicals. The primary problem with developing any large-scale industrial process based on SiO_2 is that the Si–O bonds in SiO_2 are among the strongest in nature [128 kcal (535 kJ)/mol]; consequently, efforts to activate and depolymerize SiO_2 must either overcome these high bond strengths or work around them. Carbothermal reduction is a metallurgical, brute force method that overcomes the problem. Chemical approaches that circumvent the problem have not been well explored and may offer new opportunities in silicon chemistry.[2] The approach most likely to succeed is one in which Si–O bond cleavage during SiO_2 depolymerization is matched with the formation of new, chemically equivalent Si–O bonds. In this instance, the thermodynamic requirements can be expected to be relatively modest. One alternative is the use of Na_2SiF_6, which is a byproduct of fertilizer manufacture and has been used by Corriu et al. as a starting point for the synthesis of tris(catecholato) silicates (see below) and related compounds.[3]

Reaction 1, which represents the most appropriate example of this sort of SiO_2 depolymerization, plays an important role in several industries. In addition to silicate syntheses, base-promoted SiO_2 dissolution plays a key role the synthesis of zeolites[4–6] and in the beneficiation of SiO_2 containing or contaminated minerals.[7,8] It has also been used by Kenney and Goodwin as a starting point, via esterification reactions, for the production of alkoxysilanes.[9] If it were possible to replace the inorganic base in (1) with an organic, alkoxide base, it is conceivable that this approach might provide access to new silicon-based chemicals or expand the scope of zeolite syntheses (see below) and ore beneficiation.

This conceptual approach has been explored infrequently in the literature.[10–19] Rosenheim et al. reported more than 60 years ago that silica, sand, and even quartz powder could be depolymerized in the presence of alkali catecholates (reaction 6).[10] Further work by

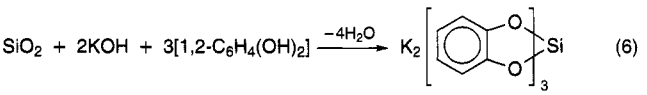

(6)

Barnum,[11] Weiss et al.,[12] Frye,[13] Boer and Flynn,[14] and Corriu[15–17] on this same reaction witnesses a recurring interest in silica activation and depolymerization. The work of Corriu et al. is the most recent, the most thorough and clearly committed to developing SiO_2 depolymerization as a chemical (rather than a metallurgical) route to Si-containing compounds.

The Corriu group was able to demonstrate that the catechol silicate complex of reaction 6 is readily elaborated by reaction with strong nucleophiles such as aryl or alkyl grignard or lithium reagents, as illustrated in the following scheme:

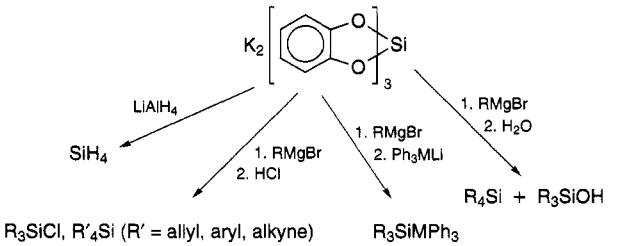

Thus, Corriu et al. have elegantly proved that it is possible to prepare organosilanes from SiO_2 without intermediate carbothermal reduction. Unfortunately, tris(catecholato) silicate is so stable that it reacts with strong nucleophiles under conditions that lead primarily to tri- and tetrasubstituted products rather than the mono- and disubstituted silanes sought by industry primarily for polymer synthesis (e.g., polysiloxane fluids and rubbers). In principle, it would be desirable to develop more reactive analogs of tris(catecholato) sili-

(3) Cerveau, G.; Chuit, C.; Corriu, R. J. P.; Gerbier, L.; Reye, C. *C.R. Acad. Sci. Paris* **1991**, *312*, *Sér. II*, 1311–15.
(4) Szostak, R.; *Molecular Sieves. Principles of Synthesis and Identification*; Van Nostrand Reinhold: New York, 1989; Catalysis Series.
(5) (a) Bibby, D. M.; Dale, M. P. *Nature* **1985**, *317*, 157–158. (b) van Erp, W. A.; Kouwenhoven, H. W.; Nanne, J. M. *Zeolites* **1987**, *7*, 286–88.
(6) (a) Qisheng, H.; Shouhua, F.; Ruren, X. *J. Chem. Soc., Chem. Commun.* **1988**, 1486–87. (b) Qisheng, H.; Ruren, X. *J. Chem. Soc., Chem. Commun.* **1992**, 168–169. (c) Herreros, B.; Carr, S. W.; Klinowski, J. *Science* **1994**, *263*, 1585–1587.
(7) Stone, R. L.; Tieman, T. D. *Soc. Miner. Engl. Trans.* **1964**, *June*, 217–222 and references therein.
(8) Tieman, T. D. *Soc. Miner. Engl. Trans.* **1964**, *Sept.*, pp 258–259.
(9) (a) Kenney, M. E.; Goodwin, G. B. U.S. Patent No. 4,717,773, Jan 1988. (b) Kenney, M. E.; Goodwin, G. B. In *Inorganic and Organometallic Polymers*; Zeldin, M., Wynne, K. J., Allcock, H. R., Eds.; ACS. Symposium Ser. 360; American Chemical Society: Washington, DC, 1988; Chapter 18. (c) Goodwin, G. B.; Kenney, M. E. *Adv. Chem. Ser.* **1990**, *224*, 251–63.
(10) (a) Rosenheim, A.; Raibmann, B.; Schendel, G. *Z. Anorg. Chem.* **1931**, *196*, 160.
(11) (a) Barnum, D. W. *Inorg. Chem.* **1970**, *9*, 1942. (b) Barnum, D. W. *Inorg. Chem.* **1970**, *11*, 1424.
(12) Weiss, A.; Reiff, G.; Weiss, A. *Z. Anorg. Allg. Chem.* **1961**, *311*, 142, 151.
(13) Frye, C. L. *J. Am. Chem. Soc.* **1964**, *86*, 3170.
(14) Boer, F. P.; Flynn, J. J.; Turley, J. W. *J. Am. Chem. Soc.* **1968**, *90*, 6973. (b) Flynn, J. J.; Boer, F. P. *J. Am. Chem. Soc.* **1969**, *91*, 5756.
(15) (a) Boudin, A.; Cerveau, G.; Chuit, C.; Corriu, R. J. P.; Reye, C. *Angew. Chem., Int. Ed. Engl.* **1986**, *25*, 473–474. (b) Boudin, A.; Cerveau, G.; Chuit, C.; Corriu, R. J. P.; Reye, C. *Organometallics* **1988**, *7*, 1165–71.
(16) (a) Corriu, R. J. P.; Young, J. C. *Chemistry of Organic Silicon Compounds*; Patai, S., Rappaport, Z., Eds.; Wiley: Chichester, 1989; Chapter 20, (b) Corriu, R. J. P. *Pure Appl. Chem.* **1988**, *60*, 99–106.
(17) Corriu, R. J. P. *J. Organomet. Chem.* **1990**, *400*, 81.
(18) Laine, R. M.; Blohowiak, K. Y.; Robinson, T. R.; Hoppe, M. L.; Nardi, P.; Kampf, J.; Uhm, J. *Nature* **1991**, *353*, 642–44.
(19) Hoppe, M. L.; Laine, R. M.; Kampf, J.; Gordon, M. S.; Burggraf, L. W. *Angew. Chem., Int. Ed. Engl.* **1993**, *32*, 287–289.

cate or different elaboration methods, in an effort to develop routes to mono- and disubstituted organosilanes. However, commercial production of these types of silanes via the direct process, e.g., reaction 3, has long been optimized in terms of yields and scales. Thus, efforts to generate organosilanes via chemically derived organosilicates are likely to be less rewarding than efforts to develop totally new chemistries based on totally new feedstocks.

We recently communicated efforts to develop saturated analogs of tris(catecholato) silicate, using ethylene glycol (EG) in place of catechol in reaction 6, wherein the products resulting from reactions with alkali metal hydroxides are the pentacoordinate species (reaction 7)[18]

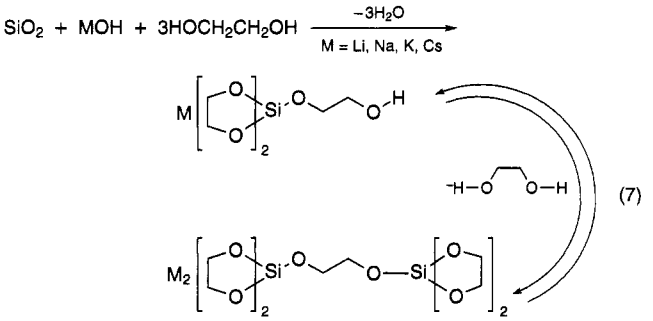

and the products obtained with alkaline earth oxides are the dianionic hexaalkoxysilicates.[19] While pentaalkoxy silicates are relatively well explored and understood,[20-29] this represents the first example of their synthesis in one step from SiO_2. In surprising contrast to the SiO_2 chemistry shown in reaction 7, GeO_2 reacts with 2,3-butanediol in the presence of the group I alkoxide, MeOK, to form a hexacoordinate complex, $K_2Ge(2,3\text{-butanediolate})_3$, rather than a pentacoordinated complex.[30]

The direct dissolution of SiO_2 in EG with alkali base provides access to a number of novel materials beginning with the set (Li−Cs) of monomeric and dimeric alkali glycolato silicates. These crystalline compounds serve as precursors to (1) phase-pure alkali silicates,[31] (2) inorganic particulates useful in electrorheological fluids,[32] and (3) by exchange with longer-chain diols, to ion-conducting polymers.[33] Furthermore, SiO_2 dissolution in basic EG is key to the nonaqueous synthesis of industrially important zeolites, e.g., ZSM-5 (silica−sodalite).[4-6] Pentacoordinate silicates are implicated as intermediates in the zeolite formation process.[6]

In the following, we present detailed studies on the synthesis and characterization of alkali pentacoordinate glycolato silicates made directly from SiO_2, including an examination of the silica dissolution process.

Experimental Section

General Procedures. All operations were carried out with the careful exclusion of extraneous moisture. Air- and moisture-sensitive materials were manipulated using standard Schlenk and glovebox techniques. All chemicals were reagent grade, purchased from standard vendors and used as received except the ethylene glycol. The EG was either used as received or recycled by distillation under N_2 before use. Classified, fused (99% purity) SiO_2 with selected surface areas and particle size distributions was donated by Minco Corp., Midway, TN. Quartzite (−350 mesh, ≈1.2 m^2/g, 98.8% pure) from Monsanto's quartzite mine in Soda Springs, ID, was a gift of Mr. Mitchell Hart. Electronics grade silica (≈7 m^2/g) was obtained from Johnson Matthey. Silica gel from several vendors was also used.

Analytical Methods. *Diffuse Reflectance Infrared Fourier Transform Spectroscopy (DRIFTS).* DRIFT spectra were recorded on a Mattson Galaxy Series FTIR 3000 spectrometer with a DTGS detector. Samples were prepared in the glovebox using random cuttings of crystalline, optical-grade KBr commercially available from International Crystal Laboratories. Approximately 600 mg of KBr was weighed out and ground in a mortar and pestle. Enough sample was weighed out to make a 0.6 wt % solid mixture. The sample was transferred to the mortar and pestle and ground with an approximately equal amount of KBr powder. The remaining KBr was added in successive portions to approximately double the amount of material and thoroughly mixed by grinding after each addition. The sample was transferred to the sample holder in the glovebox and the holder was quickly taken from the box and placed in the FTIR sample chamber, which was flushed constantly with N_2. The sample chamber was flushed for a minimum of 10 min before data collection. A minimum of 64 scans were collected for each sample at a resolution of ±4 cm^{-1}. IR peak positions were identified using a standard peak searching program.

Nuclear magnetic resonance solution studies were run on a Varian 300 MHz spectrometer at the University of Washington and a Brüker 360 MHz spectrometer at the University of Michigan. ^1H, ^{13}C, and ^{29}Si NMR spectra were taken in methanol-d_4 and referenced to TMS. Proton NMR spectra were obtained with the spectrometer operating at 300 MHz and using a 4000 Hz spectral width, a relaxation delay of 1 s, a pulse width of 82°, and 16K data points. $^{13}C\{^1H\}$ NMR spectra were obtained with the Varian spectrometer operating at 75 Hz and using a 16 000 Hz spectral width, a relaxation delay of 0.5 s, a pulse width of 60°, and 16K data points. For

(20) Chuit, C.; Corriu, R. J. P.; Reye, C.; Young, J. C. *Chem. Rev.* **1993**, *93*, 1371−1448.
(21) (a) Holmes, R. R. *Chem. Rev.* **1990**, *90*, 17. (b) Holmes, R. R.; Day, R. O.; Chandrasekhar, V.; Holmes, J. M. *Inorg. Chem.* **1985**, *24*, 2009. (c) Holmes, R. R.; Deiters, J. A. *J. Am. Chem. Soc.* **1977**, *99*, 3318. (d) Holmes, R. R.; Day, R. O.; Payne, J. S. *Phosphorus Sulfur Silicon* **1989**, *42*, 1−13. (e) Holmes, R. R.; Day, R. O.; Harland, J. J.; Homes, J. M. *Organometallics* **1984**, *3*, 347−353.
(22) (a) Kumara Swamy, K. C.; Chandrasekhar, V.; Harland, J. J.; Homes, J. M.; Day, R. O.; Holmes, R. R. *J. Am. Chem. Soc.* **1990**, *112*, 2341−48. (b) Search of the Cambridge Structural Database: Allen, F. H.; Kennard, O.; Taylor, R. *Acc. Chem. Res.* **1983**, *16*, 146. Allen, F. H.; Bellard, S.; Brice, M. D.; Cartwright, B. A.; Doubleday, A.; Higgs, H.; Hummelink, T.; Hummelink-Peters, B. G.; Kennard, O.; Motherwell, W. D. S.; Rogers, J. R.; Watson, D. G. *Acta Crystallogr.* **1979**, *B35*, 2331.
(23) Damrauer, R.; O'Connell, B.; Danahey, S. E.; Simon, R. *Organometallics* **1989**, *8*, 1167−71.
(24) Dixon, D. A.; Hertler, W. R.; Chase, D. B.; Farnham, W. B.; Davidson, F. *Inorg. Chem.* **1988**, *27*, 4012−19.
(25) Kira, M.; Sato, K.; Sakurai, H. *J. Am. Chem. Soc.* **1988**, *110*, 4599−602.
(26) Kummer, D.; Gaisser, K.-E.; Seshadri, T. *Chem. Ber.* **1977**, *110*, 1950−62.
(27) Tandura, S. N.; Voronkov, M. G.; Alekseev, N. V. *Top. Curr. Chem.* **1986**, *131*, 99−186.
(28) Cerveau, G.; Chuit, C.; Corriu, R. J. P.; Reyé, C. *Organometallics* **1991**, *10*, 1510−15.
(29) Burggraf, L. W.; Davis, L. P. In *Better Ceramics Through Chemistry II*; Mat. Res. Soc. Symp. Proc. Vol 73; Materials Research Society: Pittsburgh, PA, 1986; pp 529−42.
(30) Cerveau, G.; Chuit, C.; Corriu, R. J. P. *Organometallics* **1988**, *7*, 786.
(31) Kansal, P.; Laine, R. M. *J. Am. Ceram. Soc.* **1994**, *77*, 875−82.
(32) (a) Gamota, D. R.; Filisko, F., paper presented at ASME Fluids Engin. Conf.; June 1993. (b) Baranwal, R.; Zika, A.; Mueller, B. L.; Laine, R. M., submitted for publication.
(33) (a) Robinson, T. R. M.S.E. Thesis, University of Washington, 1990. (b) Chew, K. W.; Dunn, B.; Faltens, T.; Hoppe, M. L.; Laine, R. M.; Nazar, L.; Wu, H. K. *Am. Chem. Soc. Polym. Prepr.* **1993**, *34*, 254−55. (c) Chew, K. W.; Dunn, B.; Faltens, T.; Hoppe, M. L.; Laine, R. M.; Robinson, T. R.; Scotto, C. S., manuscript to be submitted.

the temperature-dependent studies the delay was 0.97 s. $^{13}C\{^1H\}$ NMR spectra obtained with the Brüker spectrometer operating at 75 Hz and using a 16 000 Hz spectral width, a relaxation delay of 0.2 s, a pulse width of 60°, and 16K data points. $^{29}Si\{^1H\}$ NMR spectra were obtained with the spectrometer operating at 59.6 MHz and using a 32 000 Hz spectral width, a relaxation delay of 15 s, a pulse width of 58°, and 32K data points. In some instances several mg of $Cr(acac)_3$ was added to NMR samples.

Solid-state spectra were recorded (Laboratoire de la Matière Condensée) on an MSL 400 Brüker spectrometer operating at 79.5 MHz for ^{29}Si. The spinning rate was 4 kHz. For ^{29}Si CP MAS experiments, contact times of 2 ms were used and 80 scans accumulated. A line broadening of 20 Hz was applied before Fourier transformation. Sample sizes for all solid state spectra were 300−500 mg.

Weight loss experiments were conducted using a TA Instruments TGA (Model 2950). Samples (20−40 mg), prepared as below, were placed in a platinum pyrolysis boat in dry air. Weight loss experiments were analyzed using a high-resolution (Hi-Res, setting 4) program with a maximum ramp rate of 50 °C/min to temperatures of 1000 °C. Especially moisture sensitive samples were loaded into the pan in the glovebox to avoid long exposure to the laboratory atmosphere.

Specific Surface Area (SSA) Measurements. The BET surface areas were provided by Minco, Inc., and were measured by the flow method using a Quantasorb Model QS-17 sorption analyzer. The amount of nitrogen removed from the flowing gas mixture (29.3% N_2 in He, Scott) and physisorbed on the surface was determined using a thermal conductivity detector. Accurately measured pulses (±2%) of purified N_2 (99.998%, Air Products) were used to calibrate the amount of adsorbed N_2. The BET surface area, S_g, was determined in m^2/g from

$$S_g = \left(1 - \frac{P_N}{P_O}\right)\left(\frac{A_d}{A_c}\right)4.03V_c/\text{sample mass in grams}$$

where P_N is the partial pressure of N_2 in the N_2/He mixture, P_O is the ambient pressure at 0% relative humidity (estimated from ambient pressure, $P_a + 15$), A_d is the average desorption count, A_c is the average calibration count, and V_c is the volume of the carrier gas injected during calibration. Desorption and calibration counts from three separate runs were averaged in determining S_g.

Alternately, surface areas and pore size distributions were determined by nitrogen adsorption at 77 K using the volumetric technique on a Micromeritics ASAP 2000M sorption analyzer (Norcross, GA). Samples were degassed at 110 °C for 2 h and then at 400 °C until the degas rate was less than 10 μmHg/min. The specific surface areas, SSA, were determined by the BET multipoint method with at least five data points with relative pressures between 0.001 and 0.20. Pore size distributions were determined using the density function theory (DFT) using the nitrogen on carbon at 77 K with the slitlike pores model. Analysis was done with the software package supplied with the instrument.

In addition, particle size distributions determined by laser light scattering were also provided by Minco, as discussed in the dissolution kinetics studies.

Single-Crystal X-ray Diffraction Studies. Single-crystal X-ray diffraction experiments were performed on a Siemens R3/v automated diffractometer equipped with an LT-2 low-temperature apparatus at −95 °C and graphite monochromatized Mo Kα radiation (λ = 0.710 73 Å). A colorless, irregular crystal of dimensions 0.08 × 0.15 × 0.22 mm was sealed in a thin-walled glass capillary to protect against moisture-promoted decomposition. Additional details: scan method $\theta/2\theta$, scan rate variable 2−5°/min, background to scan ratio 0.5, 2θ scan range 5−50° (h: 0/10; k: 0/15; k: **13**/13), 2126 reflections measured, merged to 1805 unique reflections, R_{int} = 0.0359, no corrections for absorption. The structure was solved by direct methods and 162 parameters were refined in a full matrix with the program SHELXTL PLUS.[34] Large thermal ellipsoids for atoms C3 and C4 indicated a slight positional disorder for these atoms which were refined isotropically at half occupancy over two positions. All other non-hydrogen atoms were allowed to refine anisotropically. Except for the hydrogens bonded to C3 and C4, all other hydrogen atoms were allowed to refine isotropically. Three reflections were excluded from refinement due to secondary extinction effects. Neutral atom scattering factors and corrections for anomalous dispersion were taken from ref 35. Table 1 contains further crystallographic details.

Table 1. Structure Determination Summary for $KSi(OCH_2CH_2O)_2OCH_2CH_2OH$[a]

compound	$KSi(OCH_2CH_2O)_2OCH_2CH_2OH$
empirical formula	$C_6H_{13}O_6Si_1K_1$
formula weight	248.35(1) amu
crystal color and habit	colorless, irregular
crystal dimensions (mm)	0.08 × 0.15 × 0.22
crystal system	monoclinic
space group	$P2_1/n$ (No. 14)
Z	4
unit cell dimensions from 25 reflections (21.1° ≤ 2θ ≤ 41.2°)	
a	7.990(1) Å
b	12.328(3) Å
c	10.519(2) Å
volume	1018.6(2) Å^3
density (calcd)	1.61(9) g/cm^{-3}
F(000)	520 electrons
linear absorption coefficient (μ):	0.63 mm^{-1}
Data Collection	
diffractometer	Siemens $R3m/v$
radiation type	Mo Kα λ = 0.710 73 Å, Lp corrected, graphite monochromator
temperature	−95 ± 2 °C
scan type	$\theta/2\theta$ scan
2θ scan range	5−50°
octants used	$+h, +k, \pm l$ (h: 0/10; k: 0/15; l: −1−3/13)
scan rate	2−5°/min, variable
scan width	0.8° below Kα$_1$ to 0.8° above Kα$_2$
background/scan ratio	0.5
standard reflections	3 measured every 97 reflections, linear decay ≫4%.
no. of data collected	2126
no. of unique reflections	1805, R_{int} = 0.0359
absorption correction	none applied
Solution and Refinement	
system used	Siemens SHELXTL PLUS, VAXStation 3500
solution	direct methods
refinement method	full-matrix least-squares
function minimized	$\sum w(\|F_o\| - \|F_c\|)^2$
hydrogen atoms	individual isotropic refinement
refined reflections with $(F_o) \geq 2\sigma(F)$	1521
no. of parameters refined	179
data/parameter ratio	8.50
$R = \sum(\|F_o\| - \|F_c\|)/\sum\|F_o\|$	0.0486
$R_w = [\sum(\|F_o\| - \|F_c\|)^2/\sum w\|F_o\|^2]^{1/2}$	0.0492
$w^{-1} = \sigma^2(F_o) + 0.00058(F_o)^2$	
GOF	1.25
mean shift/error	<0.001
maximum shift/error	0.001
secondary extinction	1.0(4) × 10^{-7}
residual electron density	+0.44/−0.43 e/Å^3

[a] A "soft" constraint on the C4 to H4B bond distance was applied during the refinement. There appears to be an intermolecular hydrogen bond interaction between H6 (glycol −OH) and O2 of the molecule related by $1/2 + x$, $1.5 - y$, $z - 0.5$ at a distance of 1.949 Å. Anisotropically refined atoms are given in the form of the isotropic equivalent thermal parameter, U(eq) defined as $^1/_3\sum_i\sum_j \mathbf{U}_{ij}a_i^*a_j^*\mathbf{a}_i^*\mathbf{a}_j$. The form of the thermal ellipsoid is $g_i = f_i \exp[-2\pi^2(U_{11}h^2a^{*2} + U_{22}k^2b^{*2} + U_{33}l^2c^{*2} + 2U_{12}hka^*b^* + 2U_{23}klb^*c^* + 2U_{13}hla^*c^*]$.

(34) Sheldrick, G. M. SHELXTL-PLUS Structure Determination Programs; Nicolet Instrument Corp.: Madison, WI, 1988.

Table 2. Powder Diffraction Patterns for Selected Monomeric and Dimeric Glycolato Silicates

dimer		monomer	
d space	*I* (rel)	*d* space	*I* (rel)
$Li_2Si_2(OCH_2CH_2O)_5$		$LiSi(OCH_2CH_2O)_2{\cdot}OCH_2CH_2OH$	
8.6653	100.0	7.0475	32.20
8.1852	41.17	6.8837	84.52
7.6885	36.76	4.4692	100.0
4.4916	20.54	4.2369	16.12
4.425	18.09	3.9056	14.84
4.3605	18.88	3.6823	20.08
4.2773	18.45	2.2073	13.18
$Na_2Si_2(OCH_2CH_2O)_5$		$KSi(OCH_2CH_2O)_2{\cdot}OCH_2CH_2OH$	
8.1852	100	8.0734	95.84
4.9241	1.90	6.9920	68.47
4.8179	2.41	6.1038	85.98
4.7539	4.09	4.8310	63.03
4.037	1.17	3.9834	55.75
3.9834	1.05	3.8554	100.0
3.8971	1.93	3.3484	81.42
$K_2Si_2(OCH_2CH_2O)_5$		$CsSi(OCH_2CH_2O)_2{\cdot}OCH_2CH_2OH$	
12.3534	6.94	10.1557	100.0
8.6232	8.72	5.8243	30.05
7.9647	5.46	4.0921	32.46
7.5255	100.0	3.6748	90.26
5.2267	25.55	3.4570	94.66
5.1513	15.16	2.7569	51.91
3.9484	6.47	2.4995	27.29
$Cs_2Si_2(OCH_2CH_2O)_5$			
10.9742	42.87		
10.4556	100.0		
10.2143	93.26		
3.7511	40.38		
3.4504	43.55		
3.4056	9.06		
3.3796	77.95		

X-ray Powder Diffraction. Data were collected for two SiO_2 samples, the glycolato silicate monomers, and dimers using a Rigaku $\theta-\theta$ wide-angle goniometer. Silica samples were packed in a glass specimen holder and placed in the goniometer. Scans were 5−80° 2θ using increments of 0.05°. The diffraction patterns for samples of 325 mesh quartzite (≈0.3 m^2/g) and a sample of Minco −50, +100 mesh, fused silica (≈43 ± 2 m^2/g) are shown in Figure 2. The quartzite peaks match exactly those of quartz, JCPDS File No. 33-1161. Powder patterns for the monomers and dimers were also recorded and the major lines are listed in Table 2.

Elemental analyses were performed by Galbraith Laboratories, Knoxville, TN.

Synthetic Procedures. All syntheses presented below, unless noted, were run using electronics grade silica from Johnson Matthey or −400 mesh silica gel. SSAs for these materials were 5−7 m^2/g. The products from all of the following syntheses were characterized per the above procedures; Tables 2−4 record the resulting data.

1. Preparation of $LiSi(OCH_2CH_2O)_2OCH_2CH_2OH$. At room temperature, 21 g (0.5 mol) of $LiOH{\cdot}H_2O$, 30 g (0.5 mol) of SiO_2, and 500 mL of ethylene glycol (EG) were added to a 1000 mL flask, and the mixture was heated to initiate distillation. The silica and LiOH slowly dissolved (1−2 h) with continuous distillation of EG and coincident distillative removal of formed H_2O. After distilling 300−350 mL of EG, the clear solution became viscous and was allowed to cool overnight. On cooling, a solid mass formed, which was broken up with a spatula and washed with 2 × 300 mL of dry, distilled ethanol. The resulting solid was then washed with 300 mL of acetonitrile, filtered, and vacuum dried at 130 °C for 1−2 h. Before drying, the product can be further purified by recrystallization from $MeOH/CH_3CN$. The yield was 92 g (0.43 mol) or 85% of theory after drying. The monomer dissolves in MeOH.

2. Preparation of $Na_2Si_2(OCH_2CH_2O)_5$. At room temperature, 53.1 g (0.25 mol) of $Na_2SiO_3{\cdot}5H_2O$, 15 g (0.25 mol) of SiO_2, and 500 mL of reagent grade EG were added to a 1000 mL flask, and the mixture was heated to initiate distillation. As the solution is heated, EG and H_2O distilled with severe frothing. *At no time was the solution observed to clear* (at lower reaction concentrations the solution remains clear). Product precipitates out coincident with silica dissolution. When 350−400 mL of EG have distilled, the solution and precipitate were allowed to cool overnight. On cooling, more solid formed. The mass was broken up with a spatula, filtered, and washed with 300 mL of acetonitrile and vacuum dried at 130 °C for 1−2 h. The yield was 60% of theoretical. More material can be isolated if the filtrate is further concentrated. The solid is poorly soluble in MeOH. Characterization of the product by TGA and FTIR indicates formation of a dimeric product that was pure (by TGA and chemical analysis) as isolated.

3. Preparation of $KSi(OCH_2CH_2O)_2OCH_2CH_2OH$ and $K_2Si_2(OCH_2CH_2O)_5$. At room temperature, 28 g (0.5 mol) of KOH, 30 g (0.5 mol) of SiO_2, and 500 mL of EG were added to a 1000 mL flask, and the mixture was heated to reflux. The silica and KOH readily dissolve with continuous distillation of EG and coincident distillative removal of H_2O. The solution became clear in 1−2 h. After approximately 350 mL of EG was removed, precipitate formed in the clear solution. The solution was then allowed to cool overnight. On cooling, a solid mass formed which was broken up with a spatula and washed with 2 × 300 mL of distilled ethanol. The resulting solid was then washed with 300 mL of acetonitrile, filtered, and vacuum dried at 130 °C for 1−2 h. Before drying, the product can be further purified by recrystallization from $MeOH/CH_3CN$. The yield was 87% of theory after drying. The dimer is prepared by heating the monomer in vacuo at 170 °C for 2−4 h. the monomer and dimer both dissolve in MeOH.

5. Preparation of $CsSi(OCH_2CH_2O)_2(OCH_2CH_2OH)$ and $Cs_2Si_2(OCH_2CH_2O)_5$. Procedures identical to those described for the preparation of the lithium glycolatosilicates were used. The yields are essentially quantitative. As isolated, the product is pure as determined by TGA, FTIR, and chemical analysis. The product can be recrystallized directly from methanol as above and dried in vacuum. Characterization of the monomeric product, is as shown in Tables 2−4. The dimeric compound is prepared by vacuum drying the monomer at 170 °C for 1−2 h. The yield is 95% of theory.

Dissolution Studies. Samples of Minco fused silica with an initial surface area of 43 ± 2 m^2/g were used to establish the rate of dissolution as a function of time and initial base concentration according to the following procedure.

Rates of dissolution as a function of time were determined using a standard reaction wherein 6.0 g (0.1 mol) of SiO_2 were mixed with 6.6 g (0.10 mol) of 88% KOH dissolved in 20 mL of EG. Then sufficient additional EG was added so that the final volume was 100 mL (1.0 M KOH). This reaction mixture was then heated, and EG was distilled at a constant rate (for all experiments) for a selected time. At the end of this time, the solution was quickly cooled and the undissolved silica was filtered off, washed with 2 × 50 mL of dry, distilled ethanol and then 50 mL of acetone, oven dried (150 °C) for 1−2 h, and then weighed. Specific surface areas (SSA) measurements on the dried samples show that the initial SSA is 43 ± 2 m^2/g; however, the SSA drops to <1 m^2/g after ≈2 h of reaction time. Efforts to measure SSAs at reaction times ≥2 h were not reproducible as none of the analytical methods used above provide reliable results for SSAs <1 m^2/g.

Rates of dissolution as a function of base concentration were determined using a standard reaction wherein 1.00 g (16.7 mmol) of SiO_2 (7.95 m^2/g) was mixed with various volumes (5, 10, 15 mL, etc.) of a stock KOH/EG solution and sufficient additional EG so that the total volume was 100.0 mL. The stock KOH/EG solution was made by dissolving 33.0 g (0.50 mol) of 88% KOH in 100.0 mL of EG (1.0 M KOH). This reaction mixture was then heated and EG was distilled at a constant rate (for all experiments) for 3 h. The resulting solution was cooled and the undissolved silica filtered off, washed successively with 2 × 50 mL of distilled ethanol, 50 mL of acetone, oven dried for 1−2 h, and then weighed.

(35) Ibers, J. A., Hamilton, W. C., Eds. *International Tables for Crystallography*; Knoch Press: Birminghanm, 1974; Vol. 4, pp 55, 99, 149.

Table 3. Ceramic Yields and Primary Decomposition Temperatures for Monomeric and Dimeric Glycolato Silicates

M glycolato silicate	monomer exp	monomer calc	dimer exp	dimer calc	dimerization temp range (°C)	decomposition temp range (°C)	DTA primary exotherm (°C)
lithium	34.1%	34.7%	40.4%	40.5%	180–240	200–340	365
sodium		39.2%	45.8%	45.3%		310–365	395
potassium	43.4%	43.2%	50.3%	49.3%	150–200	250–350	385
cesium	58.2%	58.6%	64.3%	64.6%	100–230	290–340	335

Table 4. Selected Chemical Analyses for Monomeric and Dimeric Glycolato Silicates

compound	MW	sample	C (wt %)	H (wt %)	*M* (wt %)	Si (wt %)
$LiSi(OCH_2CH_2O)_2OCH_2CH_2OH$	216.19	calc	33.33	6.06	3.21	12.99
		expt	32.50	6.20	3.03	11.20
$Na_2Si_2(OCH_2CH_2O)_5$	402.42	calc	29.85	5.01	11.43	13.96
		expt	29.53	4.93	11.53	13.91
$KSi(OCH_2CH_2O)_2OCH_2CH_2OH$	248.35	calc	29.02	5.28	15.74	11.31
		expt	28.26	5.06	14.85	11.44
$K_2Si_2(OCH_2CH_2O)_5$	434.63	calc	27.64	4.64	17.99	12.92
		expt	27.53	4.98	17.84	13.60
$CsSi(OCH_2CH_2O)_2OCH_2CH_2OH$	342.16	calc	21.06	3.83	38.84	8.21
		expt	20.72	3.63	39.38	8.58

Rates of dissolution as a function of surface area were determined using the standard reaction conditions developed for the time studies. A set of 5.0 g (83 mmol) of Minco fused silica were used with the following surface areas: 0.72 m^2/g (−120F mesh), 1.07 m^2/g (−170 mesh), 1.45 m^2/g (−270 mesh) 1.93 m^2/g (−325 mesh), 3.12 m^2/g (−400 mesh), 4.85 m^2/g (−500 mesh), and 7.95 m^2/g (−600 mesh), as determined by BET measurements (at Minco, Inc.). Particle size distributions for each sample were determined at Minco, Inc. using a Microtrac sedigraph and a Coulter laser light scattering sedigraph. The two methods of determining particle size distribution were found to provide matching data in all instances. Note that particle size distribution measurements also provide volume fractions of particles.

In these studies, the standard reaction mixture (5 g of silica and 100 mL of 1 M KOH in EG) was heated so that EG was distilled off at a slow but constant rate (for all experiments) for 6 h. The resulting solution was cooled and the undissolved silica was filtered off, washed successively with 2 × 50 mL of dry, distilled ethanol, 50 mL of acetone, oven dried (1−2 h at 150 °C), and then weighed.

Temperature Dependent Kinetic Studies. *Preparation of $KOCH_2CH_2OH$.* Solutions of $KOCH_2CH_2OH$ (1.0 M) were prepared by dissolving 0.5 mol (28.1 g) of KOH in 750 mL of EG. After dissolution was complete, H_2O and EG were distilled off under N_2 until the vapor temperature reached 198 °C and the volume was reduced to ≈500 mL. The titer of this solution was determined by titrating against an aqueous solution of potassium hydrogen phthalate with phenolphthalein as an indicator.

Minco Min-Sil 550 silica (surface area 6.25 m^2/g, Micromeritics) was used as received. Thermal analysis of this material indicated less than 0.5% loss on ignition to 1000 °C.

Kinetic Reactions. Blank runs were conducted as follows. For each reaction rate measurement, 2.000 g of SiO_2 was combined with 60.0 mL of reagent grade EG. The mixture was heated in an oil bath at 190 ± 2 °C for 1 h under N_2, distilling off any water that formed. A second set of blanks was run in an identical manner, but the mixtures were simply stirred for 10 min at room temperature. At the end of each procedure, the samples were washed with dry MeOH in a centrifuge jar. After centrifuging for 15 min, the liquid layer was decanted into a beaker. The process was repeated three times. Al foil was then placed over the tops of the jar and the beaker to keep any solvent that bumped from escaping the vessels. Each sample was then heated in a box furnace at 1 °C/min to 80 °C, held for 1.3 h, then ramped at 1 °C/min to 300 °C and held for 2 h. The heat treatment was used to remove any residual organics. The amount of undissolved SiO_2, for each reaction, was found by subtracting the initial masses of the jar (or beaker) and the foil from the final weight of the heated vessel. In both sets of reactions, the typical amounts that dissolved or remained suspended following centrifugation were <2.00 wt %. Runs were repeated a minimum of two times.

For the dissolution studies, the standard reaction solution consisted of 2.000 g (33.0 mmol) of SiO_2, added to sufficient $KOCH_2CH_2OH$ solution (typically 50.0 mL) to provide a total of 50.0 mmol of $KOCH_2CH_2OH$, to achieve a 1:1.5 Si:K ratio. The mixture was heated under N_2 in an oil bath at 160, 170, 180, 190, or 200 °C, distilling off any water formed. After a reaction time of 0.5, 1, or 3 h, the mixture was immediately cooled in a cold water bath. The samples were then treated as in the blank experiments. The mass of SiO_2 remaining was recorded for each time and temperature, and the results were used in the "onion skin" reaction rate simulation studies. All experiments were repeated a minimum of two times. Some experiments were repeated as many as six times.

Onion Skin Dissolution Kinetics Simulation. A computer analysis was performed using a set of simultaneous differential equations to simulate the dissolution process. This was necessary to determine reasonable rate constants, as the surface area of the SiO_2, and thus the reaction rate, changes greatly throughout the reaction. Minco, Inc. provided a Microtrac sedigraph analysis of the particle size distribution of the SiO_2, which divided the sample into 12 bins with particle sizes from 0.9 to 44 μm. Assuming spherical particles, the relative surface area in each bin was calculated. No allowances were made for the deviation of the particles from spherical; the surface areas from BET analysis were higher than calculated and SEMs showed that many particles were actually agglomerated finer particles. This difference affects the magnitude of the rate constant, but not its temperature dependence. Then, using the kinetic expression

$$dm^i_{SiO_2}/dt = k[\text{base}]S^i$$

where the rate of reaction of material in the ith bin is proportional to both base concentration and the surface area of the bin. Letting $k = 1$, the quantity of material removed from the particles per iteration was calculated from the resulting set of differential equations using the trapezoidal rule. New particle volumes and sizes were then calculated, and this loop was iterated 10^5 times until the simulated reaction was complete. The averages of the experimental percent SiO_2 remaining were determined for each set of reaction conditions, and these values were plotted on a graph of the simulated results. The k for the experimental data was calculated by dividing the simulated reaction time by the actual reaction time. The Arrhenius activation energy, E_a, was then calculated from a plot of ln k vs $1/T$(K). Activation parameters, $\Delta H^\ddagger$ and $\Delta S^\ddagger$ were determined similarly. Because the SiO_2 surface area was not reflected accurately by a spherical particle approximation for this particle size distribution, the reaction rates decreased more quickly than predicted.

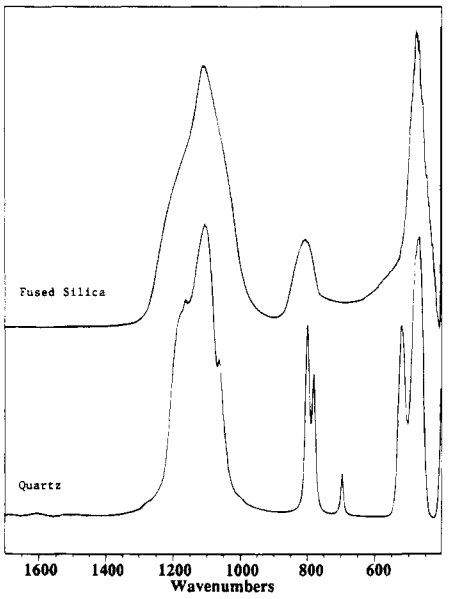

Figure 1. DRIFT spectra of amorphous (fused) silica and quartz.

Thus k decreases and E_a appears to increase for longer reaction times.

DRIFTS of silica surfaces were obtained by first heating samples of Minco 600 mesh (7.95 m^2/g) SiO_2 to 530 °C to minimize the number of hydroxyl groups on the surface. Then samples of 530 °C SiO_2 were subject to the standard reaction conditions developed for the time studies. Isolated samples were dried according to the established procedures above and stored in the glovebox until DRIFTS were run as described above. An identical sample of SiO_2 was treated under identical conditions except that the EG used contained no dissolved KOH.

Results and Discussion

The research described here can be divided into two roughly equal parts, studies on the kinetics and mechanisms of silica dissolution in KOH/ethylene glycol solutions and characterization of the resulting products. The following sections are arranged accordingly.

SiO_2 Dissolving Studies. For reaction 7 to be of practical value, the kinetics of dissolution must be reasonable; therefore, preliminary efforts were made to define SiO_2 dissolution reactivity patterns. A further motivation for these studies was to provide information pertinent to silica dissolution in EG during the synthesis of silica sodalite (ZSM-5) and related zeolitic materials.[3-5] An additional goal was to compare our results with reports on the aqueous dissolution of silica in ore beneficiation.[6,7] The first step in the kinetic studies was to determine the differences in reactivity for amorphous versus a crystalline SiO_2.

Reactivity of Crystalline and Amorphous SiO_2. Samples of SiO_2 from various sources were examined; however, for the present studies, the reactivities of three well-defined types of SiO_2 were studied in moderate detail. Thus, a sample of quartzite (325 mesh, ≈1.2 m^2/g) and two samples of fused silica [−50,+100 mesh, ≈43 ± 2 m^2/g and −35,+50 mesh, ≈0.2 m^2/g] were found by DRIFTS and XRD to be respectively crystalline and amorphous as seen in Figures 1 and 2.

The very high SSA for the 43 m^2/g sample results from a small amount of fines produced when the sample is milled without subsequent classification. In dissolution studies, these fines dissolve rapidly leaving particles with SSAs of less than 1 m^2/g to dissolve at a much slower rate. Surface areas less than 1 m^2/g are below the limit of precision of the BET setup used.

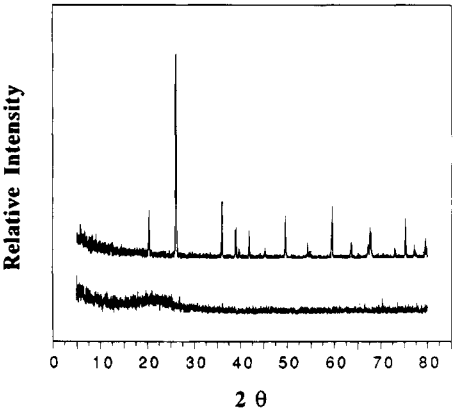

Figure 2. X-ray powder diffraction patterns of amorphous silica and quartz.

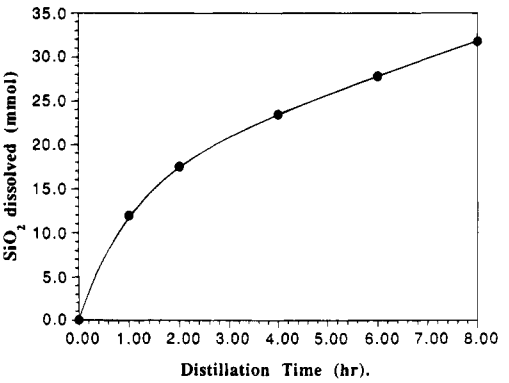

Figure 3. Dissolution of 43 m^2/g amorphous silica as a function of time. Reactions were run at 200 °C, with 6 g (0.1 mol) of SiO_2 and 100 mL of 1.0 M KOH in EG, under N_2, with minimal distillation of ethylene glycol to minimize solution volume changes.

The rate of dissolution of the 43 m^2/g fused SiO_2, as a function of time, was established using a set of standard conditions where additional EG was not added. Distillation rates were kept low to minimize superheating the reaction and to minimize the amount of EG lost. The resulting data are shown in Figure 3. Under these conditions, the 43 m^2/g surface area diminishes to ≤1 m^2/g within ≈2 h. At 8 h, more than 30 mol % of the silica has dissolved. One can use the last four points to determine that the rate of dissolution in the absence of fines is approximately 2.3 mmol/h or 0.14 g/h. Similar studies, with the 0.2 m^2/g sample, gave dissolution rates that were 1.4 mmol/h or approximately 60% the rate found for the 43 m^2/g sample, following the dissolution of fines. Under these conditions, the rate of dissolution of quartzite was quite low and not reproducible. Thus, efforts to compare the crystalline and amorphous materials were conducted using dynamic (synthetic) conditions.

The dynamic dissolution studies involved reacting 15 g of quartzite (or amorphous silica) with 1.1 equiv of KOH in 500 mL of EG under rapid distillation conditions where every 100 mL of EG distilled off was replenished. Under these conditions, after 17 h of continuous distillation (total of 1.25 L distilled off), ≈35% of the quartzite dissolves. This gives a dissolution

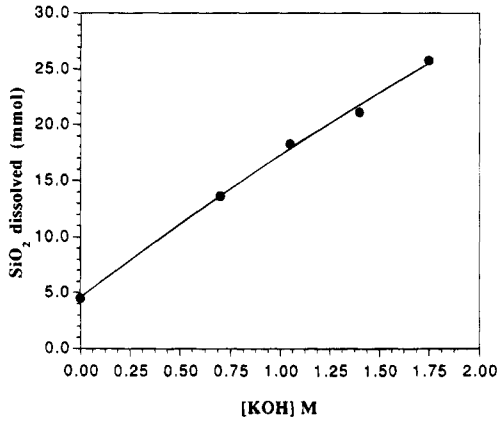

Figure 4. Dissolution of 43 m^2/g silica as a function of base concentration. Reactions were run at 200 °C, with 1 g (16.7 mmol) of SiO_2 and 100 mL of [KOH] solution, under N_2, with minimal distillation of ethylene glycol to minimize solution volume changes.

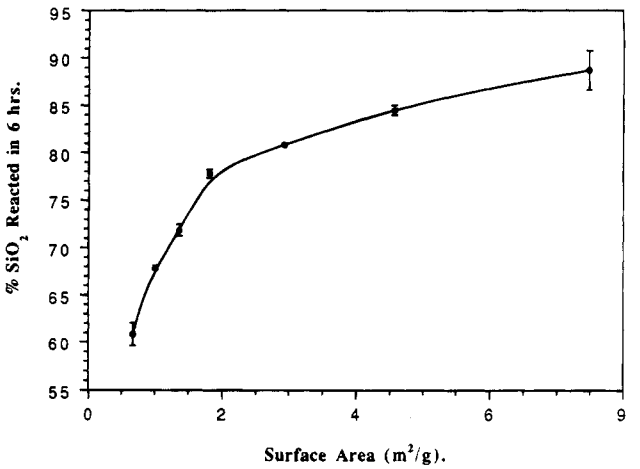

Figure 5. Dissolution of amorphous silica as a function of surface area. Reactions were run at 200 °C, with 5 g (83 mmol) of SiO_2 and 100 mL of 1.0 M KOH in EG, under N_2, with minimal distillation of ethylene glycol to minimize solution volume changes.

rate of approximately 5 mmol/h. By comparison, similar bulk studies with 43 m^2/g amorphous SiO_2 samples required 3–5 h for complete dissolution (≈50 mmol/h). Bulk studies with electronics grade silica gel (≈7 m^2/g) required <1 h for complete dissolution (>250 mmol/h). Because of the relatively slow rates of quartzite dissolution, the remaining kinetics studies were done with the 43 or 7.95 m^2/g amorphous (fused) SiO_2.

Rate of Dissolution of Amorphous SiO_2 as a Function of Base Concentration. The rate of SiO_2 (43 m^2/g) dissolution (measured as mmol/h in 3 h increments) as a function of initial base concentration was examined using the same standard conditions as used for the rate vs time studies, but with the reaction times held to 3 h. The results of these studies, shown in Figure 4, indicate that the rate of dissolution is linearly dependent on initial base concentration. The nonzero intercept was unexpected but was confirmed by running the reaction without added base. In this case, filtering off unreacted silica allowed recovery, following solvent removal, of small amounts of a clear, cross-linked polymer [presumably $Si(OCH_2CH_2O)_x$].

Rate of Dissolution of SiO_2 as a Function of Surface Area and Particle Size Distribution. The rates of dissolution of amorphous silica as a function of specific surface area (SSA) were determined using the same conditions as used for the rate vs base concentration studies, but with a constant base concentration (see experimental), a reaction time of 6 h and silica samples with well-defined SSAs and particle size distributions. The results give the curved plot shown in Figure 5. Although initially not surprising, based on the work of Tieman et al.,[7,8] it became evident that the method of plotting the results was incorrect. Given that most of the SSA (in the Figure 3 studies) is lost in the first 2–3 h, it seemed likely that a more realistic correlation of rate vs SSA would be obtained by considering only those particles actually contributing to the SSA of the individual samples. That is, the samples used for the rate vs SSA have a wide particle size distribution. Consequently, the very largest particles contribute little to the SSA on a m^2/g basis but considerably to the mass. To allow for the skewed data, the following adjustments were made.

For the 7.95 m^2/g particles, whose particle size distribution (by volume fraction) was established by two different corroborative methods (see experimental), only 20% of the particles are greater than 16 μm in size and 50% of the particles are greater than 5 μm in size. If we assume that all of the particles with sizes greater than 16 μm are spherical and not much larger than 16 μm in diameter, then these particles contribute 20% to the mass present (2.1 g/cm^3 density for amorphous silica), but calculations indicate that they actually contribute (at best) less than 0.3% of the total measured SSA of 7.95 m^2/g. If we make the same assumptions for the 50% of the particles greater than 5 μm in diameter, then these particles contribute 50% of the mass but only 3% of the total SSA. While this analysis has its drawbacks, it is clear that a plot of the fraction of particles that truly account for surface area (e.g., those <16 or 5 μm in diameter) vs degree of dissolution will provide a better estimate of the relationship than one that includes all of the mass.

Thus, Figure 6 shows plots of the percent (volume fraction) of particles less than 44, 16, and 5 μm for each silica sample, as a function of the rate of dissolution (fraction dissolved per 3 h increment, under standard conditions). The plots for the fractions of particles ≤16 and ≤5 μm in size give straight lines, whereas the plot that includes the fraction of particles ≤44 μm shows some curvature. We therefore conclude that the rate of dissolution is actually linearly dependent on the SSAs of the silica samples. The same linear dependence is found for dissolution of quartz particles in $NaOH/H_2O$ at comparable temperatures to those used here.[7,8]

Rate of Dissolution of SiO_2 as a Function of Temperature. The effect of reaction temperature on the dissolution rate was examined using standard conditions (see experimental) with data points taken for 0.5 and 1 h reaction times and a 6.25 m^2/g (by Micromeritics, −525 mesh) silica. In this study, a standard $KOCH_2CH_2OH/EG$ solution rather than a KOH/EG solution was used. Figure 7 shows a plot of the rate constant for silica dissolution vs $1/T$. As detailed in the experimental, an "onion skin" simulation was used to analyze the dissolution process and calculate rate constants as a function of temperature. The rate constants in turn allow us to calculate $E_a = 14 \pm 2$ kcal/mol for dissolution with $\Delta H^{\ddagger} \approx 11$ kcal/mol and $\Delta S^{\ddagger} \approx$

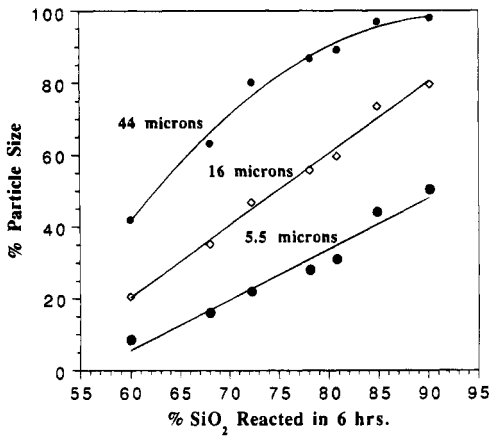

Figure 6. Dissolution of SiO_2 as a function of particle size. The plots shown are based on total volume fraction of particles of less than a specific size. The particle size distributions were determined by laser particle counting at Minco, Inc., Midway, TN. The reaction conditions are those in Figure 5. The data presented from left to right correspond to silica samples with total surface areas of 0.72, 1.07, 1.93, 3.12, 4.85, and 7.95 m^2/g. Thus, for example the 5 and 16 μm points on the right side of the graph corresponding to 90% dissolution are for the 7.95 m^2/g sample.

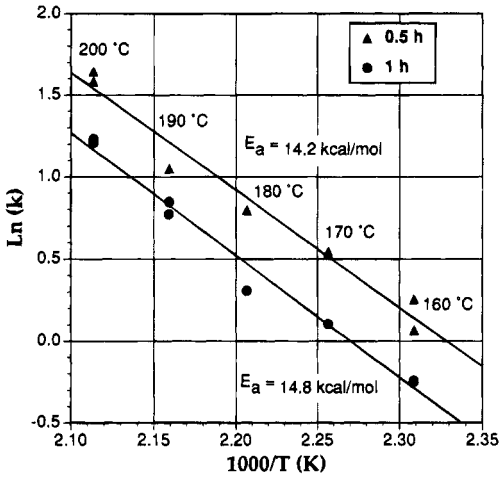

Figure 7. Arrhenius plot for SiO_2 dissolution as a function of temperature. Reactions were run in a thermostated oil bath (±2 °C, heated to selected temperatures) using 2.00 g (33.0 mmol) of SiO_2 and 50.0 mL of 1.0 M $KOCH_2CH_2OH$ in EG, under N_2, with minimal distillation of EG to minimize solution volume changes. Data obtained by simulating rate constants for dissolution as a function of temperature (see Experimental Section).

−44 cal/mol K. The E_a value is very similar to values reported for quartz dissolution in $NaOH/H_2O$, which were 15−19 kcal/mol, for the same temperature range.[7,8] The utility of these E_a, $\Delta H^{\ddagger}$, and $\Delta S^{\ddagger}$ values must be considered in the following context.

The typical dissolution reaction solution consists of KOH dissolved in EG containing suspended silica. Water must be removed to form $KOCH_2CH_2OH$, presumed to be the true reactant. The question is, "Does the initial rate of formation of $KOCH_2CH_2OH$ and coincident H_2O removal affect the dissolution rate?" To answer this, a standard reaction solution such as used in the rate vs particle size distribution studies (without SiO_2) was heated to 170 °C (to avoid coincident removal of significant amounts of EG). It was observed that nearly quantitative removal of H_2O occurs in ≈0.5 h. Thus, the active base for all of the kinetic runs (all ≥3 h and at higher temperatures) can be assumed to be $KOCH_2CH_2OH$.

Additionally, because reaction occurs well above the boiling point of H_2O, it is necessary to consider problems concerning whether or not H_2O loss from solution is rate controlling. These problems include (1) changes in H_2O vapor pressure with increasing temperature as it affects the H_2O content of the atmosphere above the solution, (2) whether or not mass transport affects the H_2O loss rate from the system, and (3) whether the solubility of H_2O in EG limits the rate of escape of H_2O. The steam tables for water[36] indicate that over the temperature range studied, H_2O vapor pressure changes nonlinearly from 6.1 atm at 160 °C to 7.8 atm at 170 °C to 15.3 atm at 200 °C. The corresponding increases in SiO_2 dissolution rates with increasing temperature are much more modest. It is likely that the vapor pressure of water above the solution does not play a role in the dissolution mechanism.

To examine the problem of mass transport, it was assumed that removal of H_2O from the still head would be the limiting factor in dissolution. To test this, one set of experiments was run with an electrically heated (heating tape) still head and the dissolution rates compared with the rates without a heated head. Therates were the same within experimental error, suggesting that dissolution is not limited by mass transport of H_2O from EG.

The concentration of H_2O in EG, under the conditions employed, can be estimated to be <0.02 wt % (0.01 M, typical analysis for reagent grade EG). This was determined qualitatively by the observation that recycled EG (distilled through a vigreux column to remove H_2O as first distilled fraction) provides faster rates of dissolution than reagent grade EG used as received. A second check comes from the above-mentioned studies on KOH transformation to $KOCH_2CH_2OH$. It is our contention that the slow step in dissolution is not determined by loss of H_2O from the reaction solution but rather loss of H_2O from the silica surface as discussed below.

Despite the above discussion, the importance of water removal from solution is still not clear; however it can be put into perspective by considering the following. In the systems studied here, conversion of silica to glycolato silicates is nearly quantitative. Yet, Bibby and Dale[5a] in their study on the synthesis of silica sodalite from amorphous silica in EG with excess NaOH make the observation that, "The water generated during the reaction of NaOH, with ethylene glycol or silica [at 150 °C] does not seem to be essential as it can be distilled off at the beginning of the reaction without affecting its progress [zeolite synthesis]." However, they note that "...no attempt was made to ensure an absolutely water-free system we cannot preclude a (catalytic) role for trace amounts of water." Similar observations were made by van Erp et al. in a related study.[5b] On the basis of our work, we can conclude that trace amounts of water are necessary to form silica sodalite and therefore detrimental to the synthesis of glycolato silicates. We can also conclude, on the basis of Bibby and Dale's and van Erp et al.'s observations, that *silica dissolution during synthesis of silica sodalite likely*

(36) *Handbook of Chemistry and Physics*, 63rd ed.; Weast, R. C., Ed.; Chemical Rubber Co.: Boca Raton, FL, 1982; pp E16−E24.

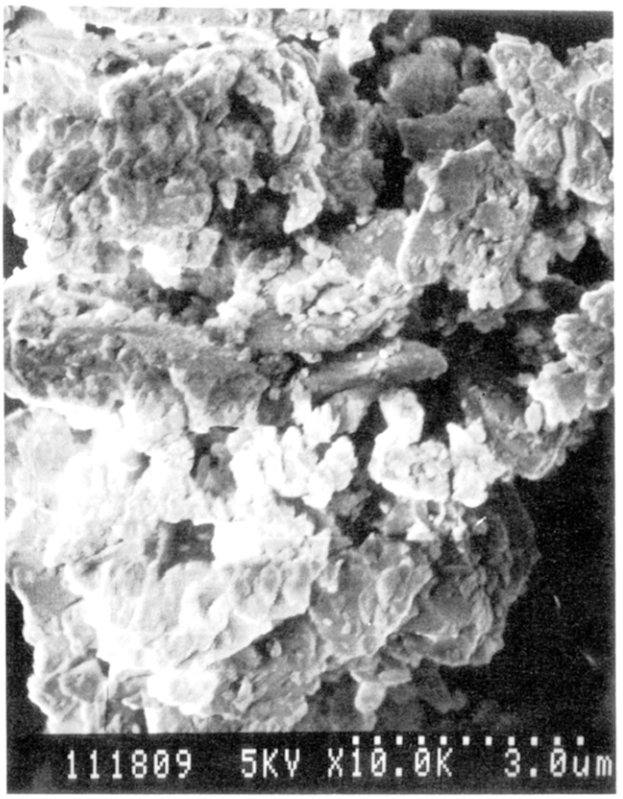

Figure 8. SEM micrograph of unreacted 7.95 m^2/g amorphous silica. Note the large dispersity of particle sizes.

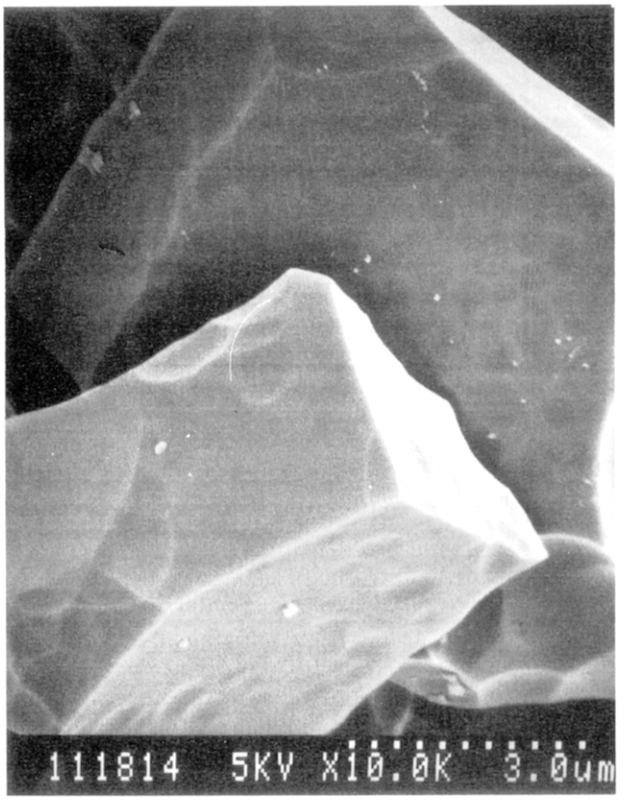

Figure 9. SEM micrograph of particles recovered from the surface area dissolution studies on 7.95 m^2/g amorphous silica. Note absence of the small particles visible in Figure 8.

involves the formation of pentacoordinate glycolato silicate intermediates. This has recently been confirmed.[6c] The possible impact of this observation on the development of new routes to zeolites remains to be seen.

Given the importance of water removal on silica dissolution and the form of the resulting products, the above observed activation energy, which defines the energy required to effect the rate-limiting step, takes on new importance if that step is formation or loss of water during reaction. To further understand the dissolution process, the silica surface was examined.

Figure 8 is an SEM micrograph of virgin 7.95 m^2/g powder. Figure 8 contrasts with Figure 9, which shows a micrograph of the 7.95 m^2/g powder particles recovered in the surface area vs dissolution rate studies following 6 h of reaction time (90% dissolution). The very fine particles are clearly missing in Figure 9. It is also important to notice that dissolution leads to smoother surfaces than are observed in the original powders. Though the surfaces are not entirely smooth (note some concavity), there is no evidence of pitting that would indicate dissolution in a highly localized fashion. Further studies were undertaken to spectroscopically characterize the particle surfaces to shed light on the dissolution process.

DRIFT Studies of Particle Surfaces. Porro and Pattacini,[37] and Blitz et al.[38] have demonstrated respectively, the utility of DRIFT spectroscopy, especially in the ν(C−H) region, for characterizing organic species on the surface of the silicate mineral, kaolin; and Cab-O-Sil. Likewise, DRIFT spectra of the O−H and C−H stretching [ν(O−H), ν(C−H)] regions provide very useful information about EG species bound to the silica surfaces.[39] To clearly define the interaction of EG with the silica surface, a sample of 7.95 m^2/g SiO_2 was heated in dry air to 530 °C for 2 h to remove any physisorbed water. The sample was then stored in a glovebox and used for a set of dissolution studies. The DRIFTS spectrum of the as-heated sample is shown in Figure 10a. The inset at the left-hand side clearly shows the trace amounts of residual Si−OH groups [ν(OH) at 3650 cm^{-1}]. No evidence is seen for the presence of physisorbed water (see below). There is a slight trace of a hydrocarbon impurity [ν(C−H) at 2942 cm^{-1}] which is ubiquitous in the FTIR at this sensitivity level.[39]

A sample of the 530 °C dried SiO_2 was heated in EG for 3 h under standard conditions (e.g., as used for the data shown in Figure 4), recovered, carefully washed, and vacuum dried at 90 °C (4 h). The vacuum drying was shown by TGA to remove any traces of physisorbed EG (<0.1 wt %). The DRIFT spectrum of this sample is shown in Figure 10b. The inset reveals the ν(O−H) and ν(C−H) region. As can be seen, the original Si−OH groups are still present. In addition, a new set of peaks appears including a broad ν(O−H) peak centered at 3280 cm^{-1} and two peaks at 2920 and 2860 cm^{-1}, which correspond to the ν(C−H) stretches in EG. Consequently, we presume, on the basis of the work of Porro and Pattacini and Blitz et al., and related work

(37) Porro, T. J.; Pattacini, S. C. *Appl. Spectrosc.* **1991**, *44*, 1170−75.

(38) Blitz, J. P.; Murthy, R. S. S.; Leyden, D. E. *Appl. Spectrosc.* **1986**, *40*, 829−31.

(39) At very high sensitivities, DRIFTS difference spectra, even of freshly prepared KBr powder, always appear to exhibit ν(C−H) peaks at 2962, 2924, and 2856 cm^{-1} which are indicative of hydrocarbon impurities either on mirrors or in the N_2 gas used to flush the compartment. In contrast, the ν(C−H) peaks for free and bound EG appear at 2944 and 2883 cm^{-1}.

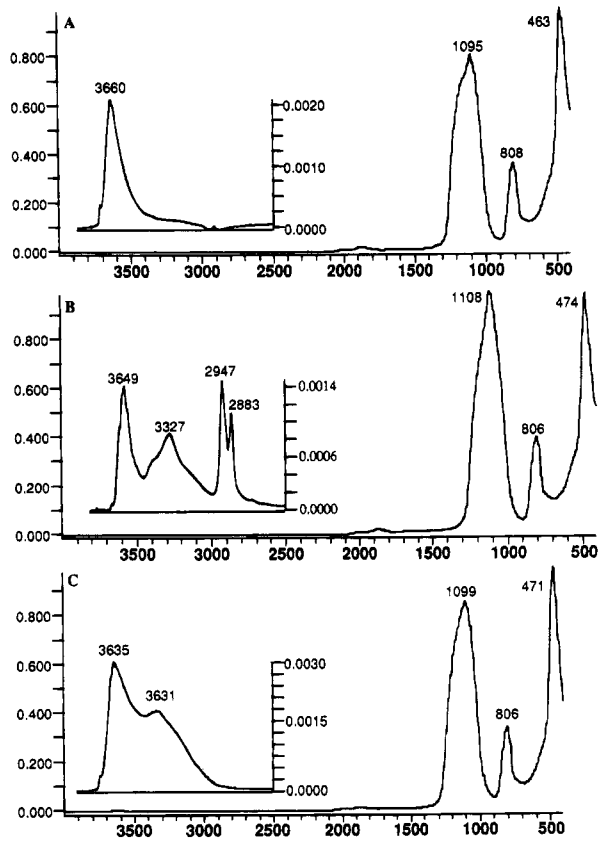

Figure 10. DRIFT spectral analysis of the surface of 7.95 m^2/g amorphous silica following exposure to ethylene glycol. (a) spectrum of 7.95 m^2/g silica heated to 530 °C for 2 h. (b) spectrum for the silica from Figure 8 heated with distilling EG for 6 h followed by drying at 90 °C in vacuo. Note the presence of bound EG as evidenced by the presence of ν(C–H) and ν(O–H) peaks. (c) Sample of Figure 8 following heating with EG/KOH under standard dissolution conditions followed by drying at 90 °C in vacuo. Note the absence of ν(C–H) peaks.

by Dubois and Zegarski,[40] that these new peaks correspond to chemisorbed EG. The presence of a new ν(O–H) peak suggests that at least some of the chemisorbed EG is monodentate, i.e., $Si-OCH_2CH_2OH$.

A similar study was run, but with a standard KOH/EG solution. After washing and drying the recovered SiO_2 sample, a DRIFT spectrum was recorded (Figure 10c). Surprisingly, the inset shows no peaks in the ν(C–H) region. However, a broad ν(O–H) peak centered at 3320 cm^{-1} is seen as well as the original ν(O–H) peak at 3650 cm^{-1}. The new peak is in the region usually associated with hydrogen-bonded hydroxyl moieties, suggesting the presence of either physisorbed water or adjacent Si–OH groups. Although, the hydrogen bonded hydroxyl groups (ν(O–H) at 3320 cm^{-1}) can be eliminated (but not the 3650 cm^{-1} ν(O–H) peak) by heating the sample to 370 °C (2 h, FTIR not shown); we do not believe that it is possible to distinguish between the two possibilities.

Another important observation can be made concerning the recovered KOH/EG SiO_2 by considering the bulk Si–O bending and stretching vibrations between 650 and 1100 cm^{-1}. These are essentially identical to the initial 530 °C SiO_2. This suggests that no potassium species remain on the SiO_2 surface. If species such as $Si-O^-K^+$ were present on the surface, a characteristic $\nu(Si-O^-K^+)$ peak at 870 cm^{-1} [31] would be clearly visible. It is not seen. No other significant peaks are found in the spectrum to indicate the presence of other potassium species.[31]

Proposed Mechanism for SiO_2 Dissolution. The information obtained from the dissolution kinetic studies and the surface chemistry studies can be summarized as follows. The rate of reaction is linearly dependent on surface area and initial based concentration. The apparent activation energy for dissolution is 14 ± 2 kcal/mol and the $\Delta H^{\ddagger}$ and $\Delta S^{\ddagger}$ values are consistent with a slow step that is associative rather than dissociative in nature. The SiO_2 surface may initially react with EG to form pendant $Si-OCH_2CH_2OH$ groups; however, these do not survive on exposure to KOH/EG at normal reaction temperatures. Furthermore, during reaction the residence time of potassium species at the surface is relatively short. Finally, in the EG/KOH dissolution system, the primary species at the surface are either adjacent Si–OH moieties or physisorbed water. With these facts in mind, it is possible to suggest a dissolution mechanism that takes them all into account, although the mechanism proposed below is only one of several possible.

We presume that the first step is formation of a pendant $Si-OCH_2CH_2OH$ species on the surface either by direct reaction as seen in the neutral studies or by nucleophilic attack of $KOCH_2CH_2OH$ on a Si center:

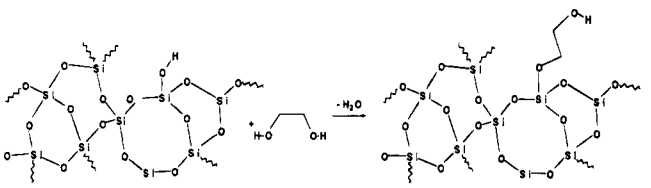

The pendant $Si-OCH_2CH_2OH$ group can aid (by hydrogen bonding) nucleophilic attack at the same Si center to form a second pendant group and simultaneously break one Si–O–Si linkage:

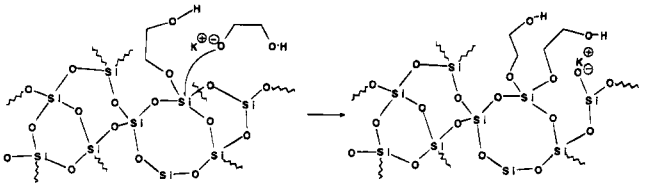

On can readily envision an unzipping mechanism wherein a series of proton transfers followed by nucleophilic attack provides ring closures, coincident with Si–O–Si bond cleavage to finally eject a neutral spirosiloxane:

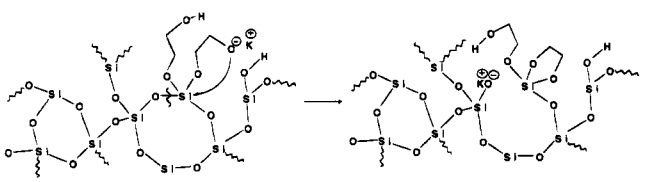

(40) Dubois, L. H.; Zegarski, B. R. *J. Am. Chem. Soc.* **1993**, *115*, 1190–91.

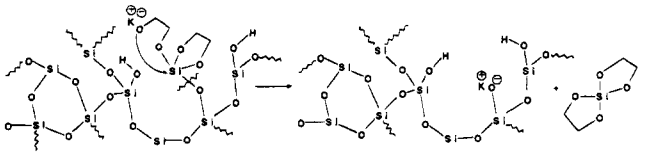

Given that the $Si-O^-K^+$ is more basic than $KOCH_2CH_2OH$ (EG $pK_a \approx 14$) and would be constantly bathed in excess EG at 200 °C, the last step is probably regeneration of the alkoxide which is then free to react with the spirosiloxane:

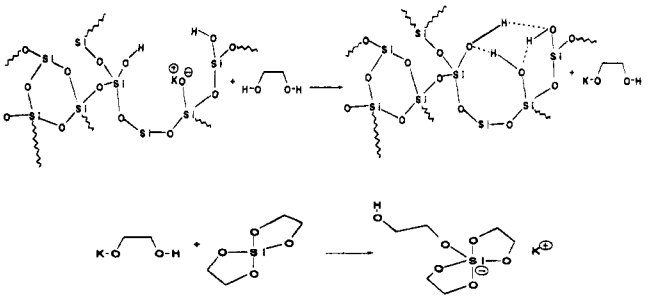

The rationale behind the proposed mechanism is as follows. The reaction is linearly dependent on both base concentration and surface area; therefore, the slow step must occur after reaction of $KOCH_2CH_2OH$ with the surface and only one $KOCH_2CH_2OH$ reacts before the slow step. The low E_a (14 kcal/mol) suggests that the slow step cannot be cleavage of a unique bond; however, the proposed "unzipping" mechanism involves a series of reactions wherein Si–O bonds are formed and broken. *There is no net change in the number of Si–O bonds*, until $KOCH_2CH_2OH$ reacts with the spirosiloxane. Thus, as noted in the Introduction, the *thermodynamic requirements of the proposed reaction mechanism can be expected to be relatively modest*. The "unzipping" process may include the slow step; although, it could also be loss of water as discussed below. Precedent for the formation of neutral alkoxysilanes from base-treated SiO_2 have been reported, albeit via gas-phase reactions.[41]

The loss of the neutral spirosilicate, followed by regeneration of $KOCH_2CH_2OH$ leaves a surface containing three adjacent Si–OH groups. These groups are capable of interacting by hydrogen bonding and their presence on the surface would account for the appearance of the broad ν(O–H) band at 3320 cm^{-1} in the KOH/EG treated SiO_2 DRIFT spectrum shown in Figure 10c. The fact that these groups are readily seen, and not $Si-OCH_2CH_2OH$ groups, suggests that they are more stable. For the process to continue, these Si–OH groups must be displaced. That is $Si-OCH_2CH_2OH$ must form. The Si–OH groups can be displaced either by self-condensation, reaction 8, or condensation with

$$Si-OH + Si-OH \xrightarrow{\Delta} H_2O + Si-O-Si \quad (8)$$

$$Si-OH + HOCH_2CH_2OH \xrightarrow{\Delta} H_2O + Si-OCH_2CH_2OH \quad (9)$$

EG as shown in reaction 9.

In either case, loss of H_2O from the surface coincides with the beginning of the first step in the dissolution cycle. This suggests that reactions 8 and/or 9 may be rate controlling rather than some event in the unzipping process. Again, the number of Si–O bonds remains the same; thus a low-energy barrier might be anticipated. Furthermore, both reactions are associative, as is the attack of $KOCH_2CH_2OH$ on the silica surface. Thus, either of the three reactions might be the slow step. However, the fact that the surface is constantly bathed in hot EG and still does not exhibit any sign of pendant $Si-OCH_2CH_2OH$ is perhaps the best argument for reaction 9 being the slow step.

Finally, the proposed reaction mechanism permits some speculation about the mechanisms of zeolite formation in the aqueous and nonaqueous synthesis of silica sodalite and related materials. If pentacoordinated intermediates do indeed play a role in the dissolution process,[6c] it is likely that their hydrolysis plays an equally important role. Given that tetraalkylammonium templates are frequently used to promote formation of particular zeolitic cages sizes and structures, we can suggest that their interaction with anionic pentacoordinated silicon centers will regioselectively control hydrolysis of the pentacoordinated silicate bonds and possibly the ensuing condensation reactions to control the structure and size of the cages that form. Support for this concept comes from the work of Hasegawa et al.,[42] who describe the nonaqueous synthesis of the 4–4 cube structure, $[Me_4N]_8[(^-OSiO_{1.5})]_8$, common to Linde A type zeolites,[4] by reaction of $Si(OEt)_4$ with Me_4NOH.

However, van Erp et al.[5b] find that for sodalite syntheses in EG, "organic templates, which are extremely effective in aqueous zeolite syntheses," have no effect. They find that EG promotes the formation of the sodalite cage and suggest that EG, which fits in the sodalite cage and is found trapped in the final product serves as a template. One could argue that in this case selective hydrolysis at one bipyramidal face (or an apex) of the glycolato silicate, followed by selective condensation at that face (apex) "forces" formation of sodalite cages, which retain EG in positions opposite hydrolyzed faces. Clearly, substantiation of this conjecture is required, perhaps through the work of Herreros et al.[6c] With these considerations in mind, we can now focus on the products that form following silica dissolution.

Synthesis of Alkali Pentacoordinate Silicates. The syntheses described in the Experimental Section are meant to be exemplary but not complete. They are all very straightforward, simple and high yield, with the exception of the sodium reactions which foam excessively. The products obtained are typically the monomers except for sodium (see below); however if these products are vacuum dried at 170 °C for several hours, they appear to convert readily to the dimers, as determined by chemical analysis. In some instances the resulting "dimers" are insoluble or sparingly soluble (in methanol). Solid-state ^{29}Si NMR studies suggest that these products are partially or fully polymerized rather

(41) Suzuki, E.; Akiyama, M.; Ono, Y. *J. Chem. Commun.* **1992**, 136–37.

(42) (a) Hasegawa, I.; Sakka, S. In *Zeolite Synthesis*; Occelli, M. L., Robson, H. E., Eds.; ACS Symp. Ser. American Chemical Society: Washington, DC, 1989; Vol.398, p 8. (b) Hasegawa, I.; Polyhedron, **1991**, *10*, 1097–1101. (c) Hasegawa, I.; Motojima, S. *J. Organomet. Chem.* **1992**, *441*, 373–380.

than dimeric, as discussed below; although, they will have the same composition as the dimers: $M_2Si_2(OCH_2CH_2O)_5$. They will dissolve in methanol in the presence of some EG, by stirring for several days. Alternately, they redissolve in hot ethylene glycol.

Initial studies focused on detailed characterization of the potassium product. These efforts were thwarted by the insolubility of the monomer in common, polar solvents including: DMF, DMSO, *N*-methylpyrrolidone, acetone, *n*-propanol, ethanol, etc. Indeed, a simple method of removing ethylene glycol from the initially recovered crystalline mass is by washing with ethanol. Surprisingly, methanol is quite effective for dissolution of all of the glycolato salts. However, efforts to recrystallize the silicate from pure methanol often lead to oils for reasons discussed below. Fortunately, addition of small amounts of glycol permits recrystallization of chemically pure products following addition of acetonitrile and/or ethyl ether. The Cs monomer is somewhat soluble in EtOH.

Stability. In general, the alkali glycolato silicates are not exceptionally moisture sensitive and can be handled in air for minutes; however, they will eventually hydrolyze and can be used to produce gels. In some instances, typically when excess base is used during the synthesis, the solid potassium salt will turn pink or red. This discoloration is readily washed away with ethanol.

In solution, the glycolato silicate ligands undergo ready exchange with other 1,2-, 1,3-, or longer chain diols simply by heating in an excess of the diol to be exchanged.[33] Details of these exchange processes will be described at a later date. Thermal stability studies, discussed below (see also ref 31), indicate that the dimeric compounds decompose in the 350–400 °C temperatures range, under N_2 (see Table 3).

Characterization. All of the alkali glycolato silicates were characterized by: elemental analysis; ^1H, ^{13}C, ^{29}Si solution and MAS solid-state NMR, powder X-ray diffractometry (Table 2), TGA, and DTA. The elemental analyses for selected compounds are presented in Table 4. The disparity in the silicon analyses is common for silicon-containing compounds that generate ceramic products on pyrolysis. Silicon analyses are often low.

Crystal Structure of $KSi(OCH_2CH_2O)_2OCH_2CH_2OH$. Figure 11 illustrates the molecular geometry and labeling scheme for the structure. Only a single orientation for the disorder of carbons C3 and C4 is shown for clarity. Atomic positional and thermal parameters are given in Table 6 in the supplementary material. Bond distances and angles are given in Table 7 in the supplementary material. The structure consists of a potassium cation and a tris(glycolato)silicate anion. The central pentacoordinate silicon is bonded to two bidentate and one monodentate glycolate ligands in a formally trigonal-bipyramidal geometry. Oxygens O1 and O4 occupy the axial positions and form the long Si–O bonds of 1.773 and 1.749 Å, respectively. O2, O3, and O5 occupy the equatorial positions at shorter Si–O distances of 1.699, 1.691, and 1.675 Å. The Si atom lies 0.04 Å below the plane defined by O2, O3, and O5. These distances are in close agreement with the Si–O bond distances found in $[(Me_4C_2O_2)_2SiO\text{-}i\text{-}Pr][K,18\text{-}C\text{-}6]$[22a] (mean $Si-O_{ax.}$, 1.744 Å, $Si-O_{eq}$, 1.688 Å) which is the only other structurally characterized five coordinate silicate containing silicon bonded to oxygen exclusively.[22b]

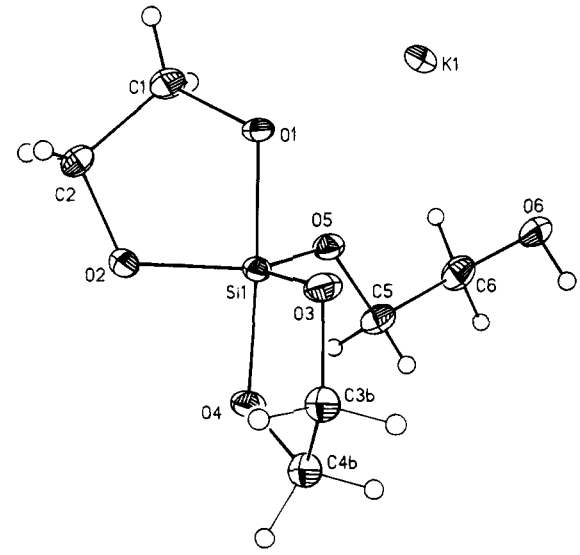

Figure 11. Ortep plot of $KSi(OCH_2CH_2O)_2OCH_2CH_2OH$. Atoms represented as 50% thermal ellipsoids.

The terminal hydrogen bonded to O6 of the monodentate glycolate ligand is hydrogen bonded to O2 (molecule related by $1/2 + x$, $1.5 - y$, $-1/2 + z$) at a H···O distance of 1.96 Å. While the Si–O2 bond distance is only marginally lengthened by this hydrogen bonding, the coordination sphere of the silicon is distorted from trigonal bipyramidal toward square pyramidal as has been seen for other five coordinate silicates which contain hydrogen bonds.[22a] Using the dihedral angle method[21c] to assess displacement, the structure is displaced 31% from trigonal bipyramidal toward square-pyramidal geometry. An additional contributing factor to this distortion may be the presence of nine O···K contacts in the range 2.72–2.90 Å.

NMR Analyses. The ^1H spectra for all of the alkali silicates were run in CD_3OD and are not particularly informative. All of the spectra exhibit a single, broad peak at 3.4–3.6 ppm in the same region as the solvent (CD_2HOD). The ^{13}C spectra of all of the alkali silicates give two peaks at 61.3 ± 0.3 and 64.3 ± 0.3 ppm. These peaks are formally consistent with the dimer shown in reaction 7 which should exhibit one peak for the bidentate glycol carbons and one for the bridging glycol carbons; however, they are not consistent with the monomer which should show three peaks. On further investigation, the peak at 64 ppm was found to correspond to free EG, even though the silicates used to prepare the NMR solutions were analytically pure. All of the glycolates appear to dissolve in CD_3OD by reacting with it (by ligand exchange) rather than by simple dissolution as demonstrated by the following study.

Figure 12 shows the variable temperature ^{13}C NMR of a sample of pure potassium monomer dissolved in CD_3OD. The two peaks for bound and free glycol are the only peaks observed in the −70 to 30 °C temperature range. We can use the ratio of these two peaks as a convenient (but approximate) measure of the relative concentration of the two species in solution. At room temperature, the peak height ratio for free EG relative to the bound EG is 0.54.[43] This ratio would be expected if the monomer dissolves and the monodentate EG exchanges with CD_3OD. As the solution is cooled to −50 °C, this ratio changes linearly (Figure 13) to 0.85. On

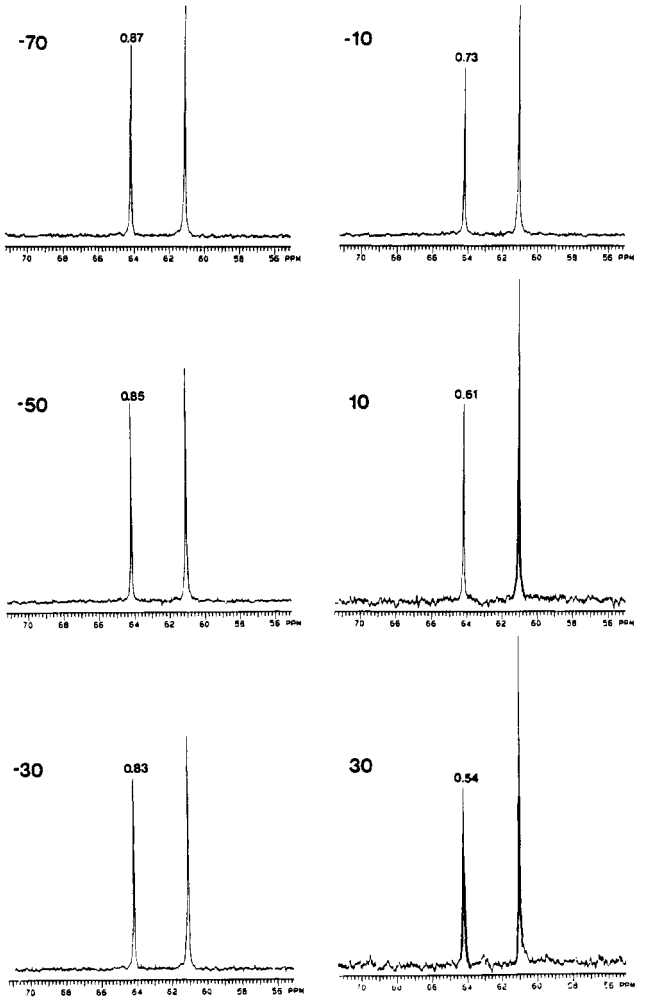

Figure 12. Variable-temperature ^{13}C NMR studies run for $K_2Si_2(OCH_2CH_2O)_5$ dissolved in CD_3OD. The ratio of the free EG peak at 64 ppm to the bound peak EG peak height at 61 ppm are noted for the various temperatures.

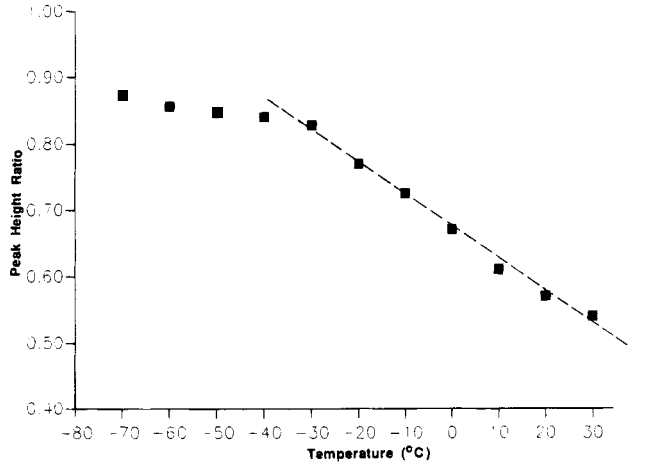

Figure 13. Ratio of free:bound ethylene glycol ^{13}C peak heights as a function of temperature (from Figure 12).[41]

warming, the ratio returns to approximately 0.50. The growth in relative amount of free ethylene glycol at lower temperature may be explained by further substitution of the bound, *bidentate* glycols. ^{13}C peaks for bound CD_3O- ligands could not be distinguished from the solvent. The following scheme suggests the likely events occurring during dissolution in MeOH:

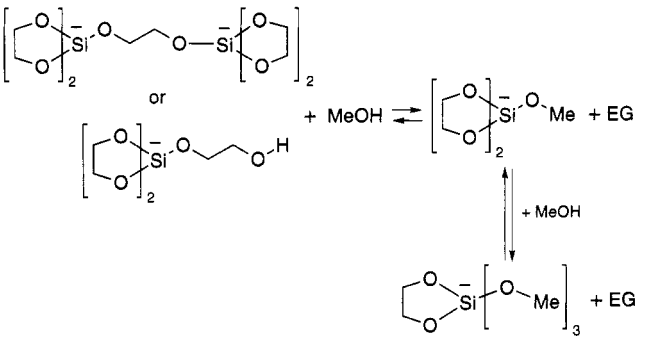

This preliminary study provides basic information on the dissolution process; although further kinetic studies are warranted, to establish the validity and thermodynamics of the steps suggested above. The observed exchange process accounts for the difficulties encountered in recrystallization of methanol solutions of the glycolato silicates, which typically oil. It also explains why added EG is necessary for recrystallization. The added EG most likely forces the exchange process back toward the monomer. The relative facility with which the glycol ligands exchange with CD_3OD clearly indicates that the glycolato silicates are much more labile than the corresponding hexacoordinate tris(catecholato)silicates.[9-14] This rapid exchange can be used to synthesize numerous diol derivatives, as will be discussed at a later date.[33]

The ^{29}Si CD_3OD solution NMRs are all quite similar. The peaks all fall in the range -103 ± 0.3 ppm, relative to TMS. The solid-state NMR spectra for dried, dimeric compounds behave somewhat similarly, in that most of the dimers exhibit the same -103 ppm peak. The implication is that the silicon magnetic environment in the solid state is nearly identical to its solution environment, for the majority of the compounds studied. These results further imply that the counterions play no role in determining the magnetic environment, only the glycolato ligands. This suggests that polymeric derivatives might offer unique ion conducting properties.[33]

However, in several instances and not always with the same ion, solid-state ^{29}Si NMR shows peaks in the region -105 to -110 ppm, e.g., the major peak for the Cs salt in Figure 14 is at -109.8 ppm.[44] A similar peak appears as an impurity in the $K_2Si_2(OCH_2CH_2O)_5$ spectrum.[44] These spectra were taken with analytically pure materials; therefore, the change in peak position cannot result from impurities. We suggest that in these cases the lower field peaks result from polymeric glycolates, $-[MSi(OCH_2CH_2O)_{2.5}]_x-$, rather than dimeric

(43) A referee has pointed out that the change in peak heights observed might correspond to the effects of temperature on T_1 values. Inversion recovery experiments allow us to determine that $T_1 = 2.0$ s for free EG and 0.75 s for bound EG. If the peak height ratios were indeed related to the effects of changes in temperature on T_1 values, one would not expect the linear dependence observed over the 60 °C (−30 to 30 °C) temperature range. Furthermore, the abrupt change in slope witnessed at temperatures below −30 °C would also not be expected. Finally, the addition of $Cr(acac)_3$ to MeOH-d_4 solutions of pure dimer at room temperature gives the same peak height ratio (within the error limits of the system) at 0.1 s delay, as found at room temperature in the variable temperature studies (0.97 s delay). This suggests that the delay time between pulses does not influence this ratio.

(44) For example, ^{29}Si MAS NMR of a sample that was primarily potassium "polymer" exhibited two peaks of approximately equal intensities at −108.1 and −108.8 ppm. A sample containing a mixture of Cs dimer and "polymer" gave peaks at −103.3 and −110.4 ppm. Babonneau, F., unpublished work.

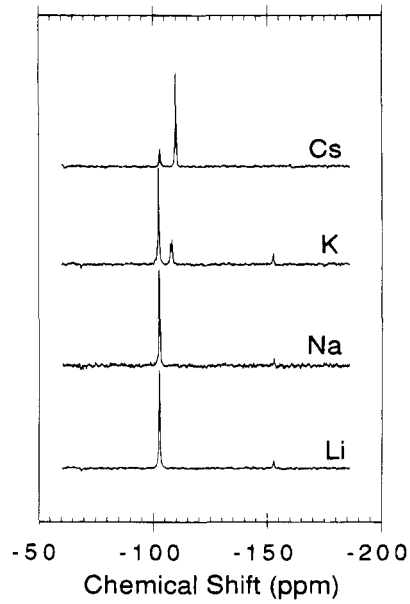

Figure 14. Solid-state MAS ^{29}Si NMRs for selected glycolato silicates. Note that the Cs peak at −109.8 ppm is shifted from the peaks of the other salts (−103 ppm), most likely because it is polymeric.

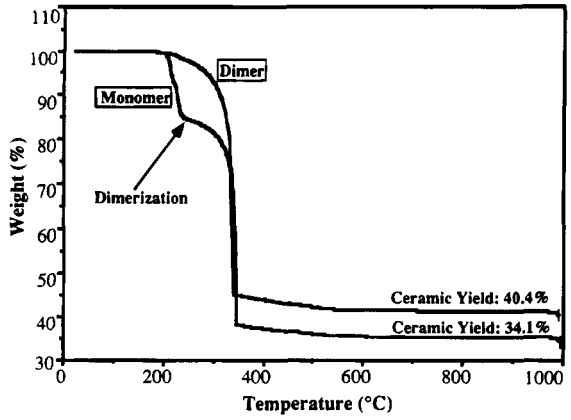

Figure 15. TGA profiles for $LiSi(OCH_2CH_2O)_2OCH_2CH_2OH$ and $Li_2Si_2(OCH_2CH_2O)_5$. Ramp rate was 20 °C/min in dry air. The peak at −92.5 ppm is the Q_3 Si in $Li_2O{\cdot}2SiO_2$. The peak at −75 ppm results from the Q_2 Si in $Li_2O{\cdot}SiO_2$.

species. As a check, the sodium salt, which precipitates as analytically pure dimer directly from solution, has a single ^{29}Si peak at −103 ppm.[6c,18] It is the only compound that does not require heating to 170 °C to effect dimerization, or "polymerization". Further support for this comes from our efforts to prepare ion-conducting polymers by substituting tetraethylene glycol for EG.[33b,c] The solution ^{29}Si NMR spectra of these compounds typically exhibit single peaks in the same region as the "polymeric species". The exact reason(s) the silicates convert one time to dimer and another time to polymer are currently unknown; although it may be a consequence of impurities including excess base or EG retained as solvent of recrystallization.

Thermal Analyses. The thermal decomposition patterns of all of the silicates were studied using X-ray powder diffractometry, diffuse reflectance IR, TGA, DTA, and ^{29}Si solid-state NMR. A brief description of the results is presented here; the details are reported elsewhere.[31] Figure 15 presents TGA profiles for the lithium silicate monomer and dimer. The initial 14% mass loss for the monomer (180−240 °C) corresponds to dimerization of the monomer wherein one monodentate EG ligand is lost for every two monomer units. The loss calculated for this process is exactly 14%. The reproducibility of the TGA data is ±1%. This weight loss is absent for the dimeric material. Both the in situ dimerized monomer and the dimer undergo significant weight loss, within the same 380−450 °C temperature range (Figure 15). The ceramic yield resulting from this decomposition is found to be 34.1%, versus a calculated value of 34.1% (Table 3). The product of pyrolysis is primarily $Li_2O{\cdot}2SiO_2$ as identified by X-ray powder diffractometry and diffuse reflectance IR.[31] Figure 16 exhibits ^{29}Si MAS NMR spectra of samples of $Li_2Si_2(OCH_2CH_2O)_5$ decomposed at selected temperatures and provides further support for the formation of $Li_2O{\cdot}2SiO_2$.[31] The peak at −92.5 ppm, at all temperatures, is indicative of a Q_3 product, as expected for $Li_2O{\cdot}2SiO_2$. The small peak at −75 ppm indicates formation of trace amounts of the Q_2 product $Li_2O{\cdot}SiO_2$, also seen in the XRD. Note that $Li_2O{\cdot}2SiO_2$ is difficult to make by other processes and is potentially useful as a high-temperature ion conductor.[31,45]

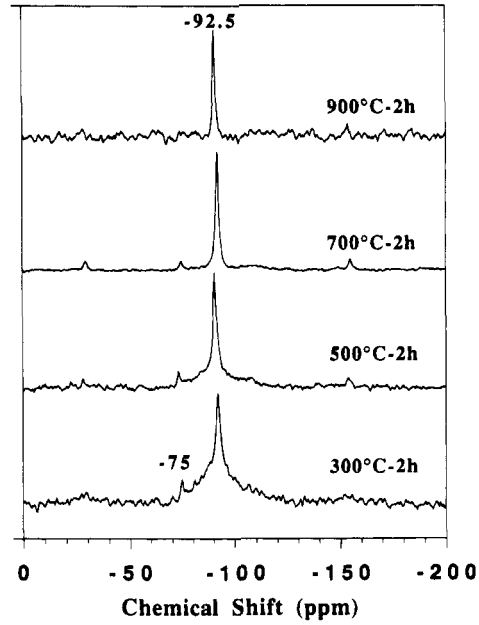

Figure 16. Solid-state MAS ^{29}Si NMR for $Li_2Si_2(OCH_2CH_2O)_5$ heated to selected temperatures. Ramp rate was 20 °C/min in dry air followed by a hold of 2 h.

The TGA profiles found in Figure 15 are representative of the decomposition patterns of all of the alkali glycolato silicate monomers and dimers. The ^{29}Si solid-state NMR in Figure 16 is representative of spectra observed for the decomposition of the other silicates; although, the potassium spectrum shows traces of a Q_3 peak at −97 ppm corresponding to small amounts of $K_2Si_4O_9$.

Conclusions

We find that SiO_2 in a wide variety of forms will dissolve readily in ethylene glycol with 1 equivalent of alkali hydroxide to produce, in essentially quantitative

(45) Szu, S.-P.; Greenblatt, M.; Klein, L. C. *J. Noncryst. Solids* **1990**, *24*, 91−100.

yield, monomeric pentacoordinate glycolato silicates containing two bidentate glycol ligands and one monodentate ligand. The dissolution reaction is first order in SiO_2 surface area and initial base concentration. E_a for dissolution is 14 ± 2 kcal/mol with $\Delta H^{\ddagger} \approx 11$ kcal/mol and $\Delta S^{\ddagger} \approx -44$ cal/mol K. These results, when coupled with DRIFTS studies on the nature of the species on the surface of the silica particles, suggest that dissolution proceeds via surface bound glycolato intermediates rather than simple attack of KOH on the surface to form silicates which then react in solution. Indeed, the critical step in dissolution is most likely the reaction of surface hydroxyls with EG to form $Si-OCH_2-CH_2OH$ species.

The fact that very high yields of glycolato silicates are obtained allows us to conclude (1) that the synthesis of zeolites under very similar conditions most likely proceeds via the formation of intermediate glycolato silicates and (2) that water content critically controls whether glycolato silicates form or silica sodalite and related zeolites. These conclusions are supported in part by work of Herreros et al.[6c]

The glycolato silicates exhibit trigonal bipyramidal geometry and appear to be completely ionic in nature. On heating, the monomers will dimerize and/or polymerize by loss of the monodentate ligand. They dissolve readily in methanol (except for the sodium derivative) but appear to do so via a ligand-exchange process wherein some of the glycolato ligands are replaced by methoxy ligands. The ligand lability of these complexes suggests that they may offer access to a wide variety of other derivatives. Finally, the glycolato silicates provide a simple and direct route to the corresponding alkali silicates glasses and ceramics, which are frequently difficult to obtain via other routes.

Acknowledgment. We thank the Office of Naval Research, the Air Force Office of Scientific Research, the Army Advanced Materials and Technology Laboratory (now Army Research Laboratories), and the Minnesota Department of Natural Resources for generous support of this work. We thank Drs. John Negrych and Jerry Snow of Minco, Inc. for helpful discussions and gifts of fused silica and virgin sand. We would also like to thank Professors R. J. P. Corriu and P. Knochel for useful discussions and suggestions. We thank Dr. Stuart W. Carr for a preprint of ref 6c. R.M.L. would like to thank Professeur Jacques Livage and the Université Pierre et Marie Curie for the award of a position as Professeur Invité and for providing accommodations and facilities during the period when this paper was written.

Supplementary Material Available: Supplementary data containing the relevant crystal structure data (12 pages); list of observed and calculated structure factors (7 pages). Ordering information is given on any current masthead page.